NPS-EC-05-005

NAVAL POSTGRADUATE SCHOOL

MONTEREY, CALIFORNIA

Analysis of Performance Characteristics of the Naval Postgraduate School MWR-05XP Mobile Weather Radar

by

Jeffrey B. Knorr

December 2005

Approved for public release; distribution is unlimited.

Prepared for: ProSensing, Inc.
107 Sunderland Road
Amherst, MA 01002-0198

THIS PAGE INTENTIONALLY LEFT BLANK

NAVAL POSTGRADUATE SCHOOL
Monterey, California 93943-5000

RDML Patrick W. Dunne, USN
President

Richard Elster
Provost

The work described in this report was funded by the Office of Naval Research through a Cooperative Research and Development Agreement (NCRADA-NPS-03-0052) between the Naval Postgraduate School and ProSensing, Inc., Amherst MA.

This report was prepared by:

_____
Jeffrey B. Knorr, Ph.D.
Professor of Electrical and
Computer Engineering

Reviewed by:

_____
James L. Kays, Ph.D.
Dean, Graduate School of Science
and Engineering

Released by:

_____
Leonard A. Ferrari, Ph.D.
Associate Provost and
Dean of Research

THIS PAGE INTENTIONALLY LEFT BLANK

REPORT DOCUMENTATION PAGE			Form Approved OMB No. 0704-0188
Public reporting burden for this collection of information is estimated to average 1 hour per response, including the time for reviewing instruction, searching existing data sources, gathering and maintaining the data needed, and completing and reviewing the collection of information. Send comments regarding this burden estimate or any other aspect of this collection of information, including suggestions for reducing this burden, to Washington headquarters Services, Directorate for Information Operations and Reports, 1215 Jefferson Davis Highway, Suite 1204, Arlington, VA 22202-4302, and to the Office of Management and Budget, Paperwork Reduction Project (0704-0188) Washington DC 20503.			
1. AGENCY USE ONLY *(Leave blank)*	**2. REPORT DATE** December 2005	**3. REPORT TYPE AND DATES COVERED** Technical Report for the period 1 OCT 03 – 31 DEC 05	
4. TITLE AND SUBTITLE: Title (Mix case letters) Analysis of Performance Characteristics of the MWR-05XP Mobile Weather Radar			**5. FUNDING NUMBERS** N6227103WER0026
6. AUTHOR(S) Jeffrey B. Knorr			
7. PERFORMING ORGANIZATION NAME(S) AND ADDRESS(ES) Naval Postgraduate School Monterey, CA 93943-5000			**8. PERFORMING ORGANIZATION REPORT NUMBER** NPS-EC-05-005
9. SPONSORING /MONITORING AGENCY NAME(S) AND ADDRESS(ES) ProSensing, Inc. 107 Sunderland Road Amherst, MA 01002			**10. SPONSORING/MONITORING AGENCY REPORT NUMBER**
11. SUPPLEMENTARY NOTES The views expressed in this report are those of the author and do not reflect the official policy or position of the Department of Defense or the U.S. Government.			
12a. DISTRIBUTION / AVAILABILITY STATEMENT Approved for public release; distribution is unlimited.			**12b. DISTRIBUTION CODE** A

13. ABSTRACT (maximum 200 words)

In 1998, the Naval Postgraduate School (NPS) Center for Interdisciplinary Remotely Piloted Aircraft Studies (CIRPAS) and the NPS Department of Electrical and Computer Engineering (ECE Dept.) collaborated on the acquisition of a mobile radar, the AN/MPQ-64 (Sentinel). This is a modern X-band, pulse Doppler radar used by the Army for forward area air defense. An SBIR project funded by the Office of Naval Research resulted in a contract to ProSensing, Inc., Amherst, MA to retrofit this radar with a weather processor. The intent is to provide a military capability to assess battlespace weather in real time. This capability will be developed using the NPS radar as a testbed. When the weather capability has been fully implemented on the NPS radar, it will also have application as a scientific instrument for severe storm research because of its mobility and cutting-edge capabilities. The modified radar has been designated the MWR-05XP (Mobile Weather Radar, 2005, X-band, Phased Array).

This report presents the results of an analysis of numerous aspects of the radar's performance as a weather sensor. The ability of the MWR-05XP radar to detect rain with different levels of reflectivity, the ability of the radar to detect clear air turbulence with different structure parameters and echoes from birds and insects has been examined. Curves are provided to determine correlation and decorrelation times for weather signals with varying rms velocity spread. MWR-05XP post detection integration improvement has been computed for a Rayleigh weather target with varying pulse-to-pulse correlation and curves are provided to determine the improvement in terms of the number of pulses integrated. Lastly, scan strategy is discussed with emphasis on obtaining weather signal parameter estimates with small variance while at the same time achieving a rapid volumetric update rate. Electronic scan is the feature that enables the radar to achieve a rapid volumetric update rate. Data quality control is also discussed.

14. SUBJECT TERMS X-band, mobile weather radar, electronically scanned weather radar			**15. NUMBER OF PAGES** 51
			16. PRICE CODE
17. SECURITY CLASSIFICATION OF REPORT Unclassified	**18. SECURITY CLASSIFICATION OF THIS PAGE** Unclassified	**19. SECURITY CLASSIFICATION OF ABSTRACT** Unclassified	**20. LIMITATION OF ABSTRACT** UL

NSN 7540-01-280-5500

Standard Form 298 (Rev. 2-89)
Prescribed by ANSI Std. 239-18

THIS PAGE INTENTIONALLY LEFT BLANK

ABSTRACT

In 1998, the Naval Postgraduate School (NPS) Center for Interdisciplinary Remotely Piloted Aircraft Studies (CIRPAS) and the NPS Department of Electrical and Computer Engineering (ECE Dept.) collaborated on the acquisition of a mobile radar, the AN/MPQ-64 (Sentinel). This is a modern X-band, pulse Doppler radar used by the Army for forward area air defense. An SBIR project funded by the Office of Naval Research resulted in a contract to ProSensing, Inc., Amherst, MA to retrofit this radar with a weather processor. The intent is to provide a military capability to assess battlespace weather in real time. This capability will be developed using the NPS radar as a testbed. When the weather capability has been fully implemented on the NPS radar, it will also have application as a scientific instrument for severe storm research because of its mobility and cutting-edge capabilities. The modified radar has been designated the MWR-05XP (Mobile Weather Radar, 2005, X-band, Phased Array).

This report presents the results of an analysis of numerous aspects of the radar's performance as a weather sensor. The ability of the MWR-05XP radar to detect rain with different levels of reflectivity, the ability of the radar to detect clear air turbulence with different structure parameters and echoes from birds and insects has been examined. Curves are provided to determine correlation and decorrelation times for weather signals with varying rms velocity spread. MWR-05XP post detection integration improvement has been computed for a Rayleigh weather target with varying pulse-to-pulse correlation and curves are provided to determine the improvement in terms of the number of pulses integrated. Lastly, scan strategy is discussed with emphasis on obtaining weather signal parameter estimates with small variance while at the same time achieving a rapid volumetric update rate. Electronic scan is the feature that enables the radar to achieve a rapid volumetric update rate. Data quality control is also discussed.

(Back to Table of Contents)

THIS PAGE INTENTIONALLY LEFT BLANK

EXECUTIVE SUMMARY

Theoretical results provided in this report predict the performance of an electronically scanned X-band radar equipped with a weather signal processor. The radar is the MWR-05XP (**M**obile **W**eather **R**adar, 20**05**, **X**-band, **P**hased array). The single pulse average power return from precipitation, birds, insects, flocks of birds, swarms of insects and clear air (turbulence & wind shear) has been investigated. A postdetection integration gain curve keyed to the MWR-05XP is provided along with a curve of single pulse fluctuation loss. Integration gain curves for weather signal samples with correlation values from 0.40 to 0.99 are provided. These curves quantify integration gain as a function of the number of pulses integrated taking signal fluctuation and pulse-to-pulse correlation into account. Lastly, an optimum sampling strategy is proposed. The proposed strategy maximizes the volumetric update rate while simultaneously minimizing the variance of signal parameter estimates.

The MWR-05XP is designed for a maximum operational range of approximately 75 km. A PRF of 2 kHZ is required to achieve an unambiguous range of 75 km. For the operating frequency range of the MWR-05XP, this PRF results in an unambiguous velocity of about 30 m/s. Increasing PRF to the system limit, 10 kHz, increases the unambiguous velocity to about 150 m/s while unambiguous range drops to 15 km. The latter limits are well suited for use of the MWR-05XP as a weather research instrument where the radar would probably be positioned to observe severe weather at short range. The former limits would be suitable for integration of an ordinary weather observation capability into the normal military operational mode of the radar.

Single pulse received signal power for precipitation has been computed for reflectivity levels between 5 dBZ and 75 dBZ and ranges from 5 to 45 km. These computations show average echo signal power is generally in the range between the system noise floor and receiver saturation level. The reflectivity range 5 – 50 dBZ corresponds to rainfall rates of approximately 0.06 – 37.7 mm/hr. Larger reflectivities are likely due to melting ice. The results show observation of severe weather with high reflectivity at short range is likely to cause receiver saturation. Even for reflectivities with average power return below saturation, individual pulses may drive the receiver into saturation as they can typically exceed the average by as much as 10 dB.

In the absence of precipitation, return can be observed from birds, insects and clear air. Computations show the X-band, single pulse echo signal power from individual birds and large insects such as moths will lie above the system noise floor if range is less than about 10 km. Flocks of birds and insect swarms produce a much greater return with average power very similar to that for echoes from precipitation. In fact, research has shown that “clear air” return is frequently associated with insects and has a diurnal pattern. Birds, although they are targets with larger cross-section, are not as numerous so their RCS density is generally less than that of insects.

True clear air return results from variations in refractive index due to turbulence and wind shear. Turbulence is the predominant mechanism. The return from clear air turbulence is weak, however, and computations show single pulse echo signal power is typically more than 20 dB below the MWR-05XP system noise floor even for strong turbulence. Thus, it will not normally be a factor.

If clear air turbulence is of interest, the signal can be processed if a sufficiently long observation time is used. Computations show strong turbulence at a range of 10 km produces a single pulse echo signal with power $\overline{P_r} \approx -134$ dbm in X-band. An integration gain of 21 dB would bring this signal to the system noise floor and further integration would produce SNR > 0 dB so the signal could be detected. Several thousand pulses would be required and this would consume a time on the order of one second for each beam position. A time on the order of minutes would be required to scan a frame of reasonable size. For reference, the S-band WSR-88D NEXRAD radar displays clear air reflectivity between –28 dBZ and +28 dBZ using a 10 minute observation time for its volume scan. The volume scan covers 360 degrees in azimuth and 0.5 to 4.5 degrees in five elevation beam steps. The lowest two elevation angles are scanned twice using different pulse widths and PRFs for reflectivity and velocity.

Pulse integration can be used as desired to improve signal-to-noise ratio, SNR. The signal from precipitation is noncoherent on a relatively short time scale so noncoherent integration must be used. Albersheim's equations have been used to model the noncoherent integration gain, G_{nc}, for an arbitrary number of integrated pulses. The result also depends on detection and false alarm probabilities. $P_d = 0.95$ and $T_{fa} = 1$ hour have been chosen as reasonable for the MWR-05XP. For this choice of parameters, integration of 500 pulses produces a noncoherent integration gain, $G_{nc} = 19$ dB.

Precipitation is a Rayleigh target, the observed radar cross-section is exponentially distributed and thus echo signal power varies with time. The echo signal power for any particular pulse might be significantly less than the average echo signal power. There is a resulting fluctuation loss that impacts single pulse detection probability. This fluctuation loss has been modeled using Shnidman's equations. For a single pulse detection probability $P_d = 0.95$ the fluctuation loss is 12 dB. For a single pulse detection probability $P_d = 0.99$ the fluctuation loss is 17.9 dB. This loss must frequently be overcome by using integration.

Work by Kanter showed there will be a reduction in fluctuation loss if pulses are integrated. The reduction in fluctuation loss when integrating *n* pulses can be modeled using an equivalent number of pulses, n_e, that depends on correlation coefficient. Computations have been carried out and results show that when correlation coefficient $\rho \geq 0.4$, the effective number of pulses is less than the actual number. As $\rho \to 1$ (pulses completely correlated) the effective number of pulses, $n_e \to 1$.

Integration improvement can be expressed in terms of integration gain and fluctuation loss for pulses with arbitrary correlation coefficient. Computations have been carried out and curves are provided that quantify the integration improvement for correlation coefficients ranging from $\rho = 0.4$ to $\rho = 0.99$. These curves show that if a sufficient number of pulses are integrated, the effect of weather target cross-section fluctuations is masked. The integration improvement approaches that for a non-fluctuating target with RCS $\sigma_{avg} = E\{\sigma\}$.

The last issue considered in this work was optimum sampling strategy. Weather radars typically produce estimates of the first three Doppler moments of the weather signal; reflectivity, average radial velocity and radial velocity spread. The estimates have a variance that depends on the number of samples averaged and their correlation coefficient, ρ. For a given number of samples, $\rho = 0$ yields the estimate with minimum variance. An optimum sampling strategy is defined here as one that maximizes the volumetric update rate while simultaneously minimizing the variance of the weather signal parameter estimates.

Reflectivity is estimated from the average power return. Average radial velocity is estimated using the average of phase shifts computed between pulse pairs (the pulse pair algorithm). Pairs of pulses must be coherent (highly correlated) and therefore closely spaced in time to unambiguously compute velocity from the inter pulse phase shift. However, pulse pairs should be widely spaced in time if successive power and velocity estimates are to be independent (uncorrelated).

The Doppler spectrum of a weather signal is assumed Gaussian with spectral spread directly tied to weather target rms velocity spread, σ_v. The correlation coefficient of the signal is found from the Fourier transform of the power spectral density. Therefore, the correlation coefficient of the signal is also Gaussian. The correlation coefficient for an X-band weather signal has been computed for a typical range of rms velocity spreads, $0.1 \le \sigma_v \le 10$ m/s. The correlation coefficient has been used to determine the time the X-band signal remains correlated as well as the time required for the signal to decorrelate. These times determine the maximum acceptable spacing between pulses in a pair and the time one must wait to obtain another independent sample pair from the same resolution cell.

An optimum sampling strategy follows from the above considerations. A pair of pulses should be transmitted to collect a single sample pair for each resolution cell of interest in a beam position. The process is repeated for each of the beam positions in a frame. After sample pairs have been collected for all beam positions in a frame, the elapsed time should exceed the weather signal decorrelation time and the process can be repeated to collect an independent set of sample pairs.

Implementation of the optimum sampling strategy requires electronic antenna beam scan. Sample time for a beam position is determined by the spacing between pulses in a pair and the time required to electronically switch beam positions. The time required for the

MWR-05XP to switch beam positions is nominally 100 μs. At the maximum PRF of 10 kHz, the correlation of adjacent pulses is high and the time between pulses is 100 μs, the same as the nominal phase shifter switching time. The total time required to collect a sample pair and switch beam positions is thus 300 μs. Sample pairs could be collected from 200 beam positions, for example, in 60 ms. After 60 ms has elapsed, the weather signal decorrelates and another scan of the frame yields independent sample pairs. Unambiguous range for this scenario would be 15 km.

It is shown that the sampling strategy described above allows for simple control of data quality. The desired variance of a parameter estimate can be specified and since samples are independent, the number of samples required can be easily determined. Collecting the computed number of samples with sufficiently high SNR then results in weather signal parameter estimates with known variance. In the case of reflectivity, however, the radar must be accurately calibrated so echo signal power at the receiver input can be determined from the observable I and Q channel output voltages. Each dB of calibration error will bias the reflectivity estimate by one dBZ.

(Back to Table of Contents)

ACKNOWLEDGEMENTS

As with any major project, there are numerous individuals who have contributed to the final product, a mobile, electronically scanned radar with a weather processing capability. Much of the work described here would not have been undertaken or even possible without them. The original requirement for a mobile radar to track UAVs was brought to the author by Bob Bluth, Executive Director of the NPS CIRPAS Research Center in 1998. This led to a collaborative effort to obtain a radar that would serve the needs of both CIRPAS and the NPS Department of Electrical and Computer Engineering. Paul Buczynski, Staff Director of the NPS ECE Department Radar Laboratory, was assigned the task of identifying radars that might meet the CIRPAS tracking requirement. Bob and Paul made the subsequent contacts that led to acquisition of a surplus radar. Bob conceived of the idea to modify the radar by adding a weather processor. ProSensing, Inc., developed the weather processor with funding provided through the Office of Naval Research SBIR Program. Ivan Pop-Stefanija led the ProSensing work on the weather processor and Paul Buczynski attended to the metamorphosis of the radar from its original operational configuration to its current physical configuration. The author focused principally on the analytical work related to the system's performance as a weather radar. Work carried out at the Naval Postgraduate School was funded through a Cooperative Research and Development Agreement (CRADA) with ProSensing. Ken Johnson at Raytheon also provided invaluable assistance. Ken answered many questions about the radar that arose during the course of the project and Raytheon, under contract, provided a device to control the radar. Danielle Kuska, NPS Director of Research Administration, prepared the Cooperative Research and Development Agreement and two subsequent Amendments. Without the contributions of all these individuals, the weather radar described in this report would not exist and the author would not have had the opportunity to work on this interesting and stimulating project.

(Back to Table of Contents)

THIS PAGE INTENTIONALLY LEFT BLANK

TABLE OF CONTENTS

THIS PAGE INTENTIONALLY LEFT BLANK

LIST OF FIGURES

LIST OF FIGURES (CONTINUED)

(Back to Table of Contents)

LIST OF TABLES

(Back to Table of Contents)

THIS PAGE INTENTIONALLY LEFT BLANK

I. INTRODUCTION

A. BACKGROUND

The Naval Postgraduate School (NPS) Department of Electrical and Computer Engineering (http://www.nps.navy.mil/ece/), the NPS CIRPAS Research Center (http://web.nps.navy.mil/~cirpas/) and ProSensing, Inc. (http://www.prosensing.com/) have collaborated on the development of a mobile, phased array, pulse Doppler weather radar. The system was created from an AN/MPQ-64 mobile radar obtained from the Army (Figure 1). A Weather Radar Processor (WRP) was developed by ProSensing, Inc. (http://www.prosensing.com/) under a Phase II SBIR project (Topic N01-035) funded by the Office of Naval Research (ONR). The weather processor was added to the radar and the radar was mounted on a flatbed truck (Figures 2, 3).

NPS has a Cooperative Research and Development Agreement with ProSensing, Inc. and has been collaborating with ProSensing on research related to the future operational use of the radar as a weather instrument. In keeping with the nomenclature applied to the National Weather Service NEXRAD radars (WSR-88D, Weather Surveillance Radar, 1988), the author has designated the radar described in this report the MWR-05XP (Mobile Weather Radar, 2005, X-band, Phased Array). The radar can be electronically scanned and it is this feature that gives it a unique capability as a weather research instrument. That capability is rapid volumetric update of weather signal parameter estimates while simultaneously achieving small variance of the estimates. (Back to Table of Contents)

B. OBJECTIVE

The objective of the work described herein was to investigate a number of issues related to the operation of the MWR-05XP as a weather sensor. These included range and velocity ambiguity, sensitivity, return from precipitation, clear air return, bird and insect return, fluctuating target integration improvement and scan strategy. This report should serve as a useful reference on the performance of the MWR-05XP. (Back to Table of Contents)

C. APPROACH

The approach throughout is analytical and builds on existing theory to develop results specific to the operation of the MWR-05XP as a weather sensor. Basic radar system measurements were made to support the analysis; Appendix 2. (Back to Table of Contents)

D. RELATED WORK

There is a significant body of literature relating to the use of radar for weather measurements. Much of this relates to the WSR-88D NEXRAD weather radar.

Figure 1. MWR-05XP (Mobile Weather Radar-2005, X-band, Phased Array). Radar shown in its original military operational configuration, mounted on a trailer. (Back)

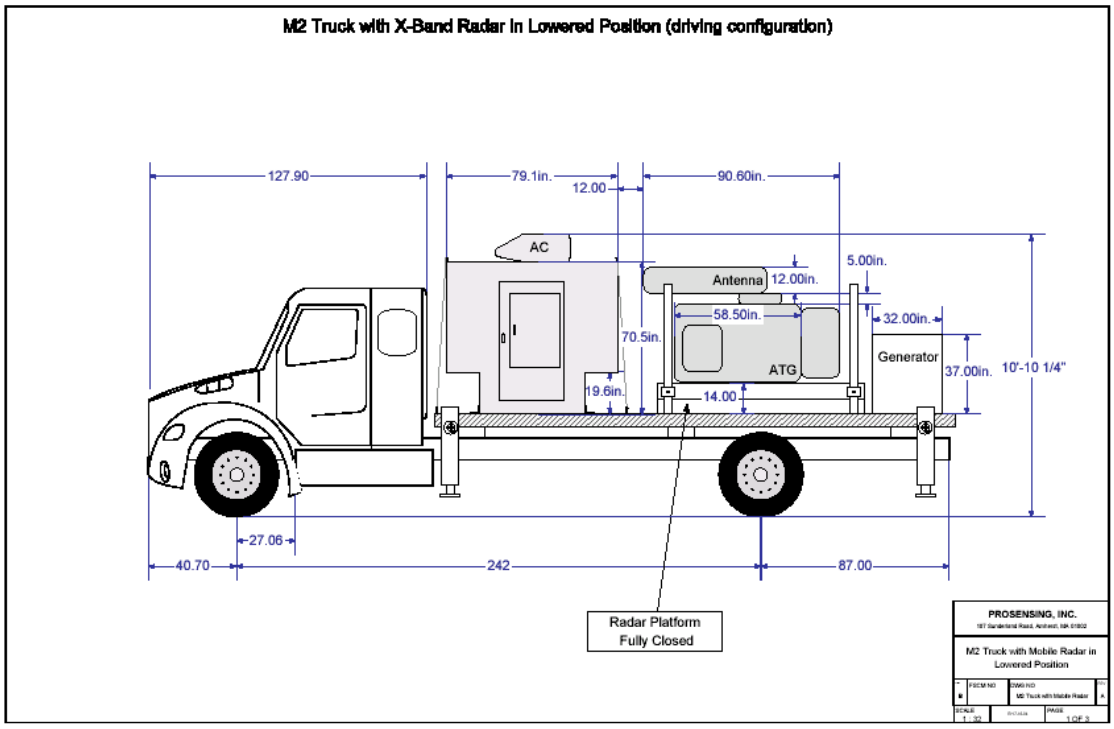

Figure 2. Drawing showing MWR-05XP radar mounted on a flatbed truck with 400 Hz diesel generator and operators' shelter. Antenna is in stowed position. Radar is mounted on a platform used to raise the radar above the operator's shelter when in use. Courtesy ProSensing, Inc. (Back)

Figure 3. Photograph of MWR-05XP mobile weather radar shown with radar platform raised for operation. The main 400 Hz diesel generator on the rear of the truck powers the radar. A 120 V, 60 Hz generator on the driver's side below the truck bed provides power for computers and equipment in the operator's shelter. (Back)

There are approximately 160 NEXRAD radars that provide coverage of the continental US, Alaska, Hawaii, Guam and Puerto Rico. These radars can be accessed on the internet using the URL (http://weather.noaa.gov/radar/national.html). Doppler radar theory and meteorology are described in Ref. [1]. A rigorous treatment of Doppler radar and weather observations can be found in the text by Doviak and Zrnic, Ref. [2]. Other texts covering weather radar theory include Sauvageot, Ref. [3], and Rinehart, Ref. [4]. Skolnik, Ref. [5], also discusses radar return from weather as well as land clutter, sea clutter, bird and insect return. Surface return is clutter for a weather radar but that problem is not treated here. Martin [6] has investigated return from birds and insects. Others [7] – [12] have published work related to the detection of radar targets and in particular, the detection of signals from fluctuating targets such a precipitation. These theoretical results have been used to predict the performance of the MWR-05XP weather radar and to determine temporal and spatial sampling strategies that fully exploit the electronic scan capability of the radar. (Back to Table of Contents)

II. ANALYSIS OF MWR-05XP PERFORMANCE

A. WEATHER RADAR EQUATION

The weather radar equation can be found in various forms in a number of sources (Refs. [1] – [5]) and will not be derived here. The average single pulse return echo signal power from precipitation is given by

$$\overline{P_r} = \frac{P_t G_t^2 \lambda^2 \left(\theta_B \varphi_B / \pi^2\right)(c\tau)}{1024 \ln(2) R^2 L_s} \frac{\pi^5 |K|^2}{\lambda^4} Z \qquad (1)$$

where

$\overline{P_r}$ = average received echo signal power in Watts
P_t = transmit power in Watts
G_t = transmit/receive antenna gain
λ =wavelength in meters
θ_B = antenna 3 dB elevation beamwidth
φ_B = antenna 3 dB azimuth beamwidth
$c = 3 \times 10^8$ m/s
$|K|^2 = \left|(\varepsilon_r - 1)/(\varepsilon_r + 2)\right|^2 \approx 0.93$ (water)
R = range in meters
L_s = system loss
Z = reflectivity in mm^6/m^3.

The nature of a weather target is such that pulses are normally integrated noncoherently (post-detection). If pulses are integrated, then an integration gain factor, $G_{nc}(n)$ and fluctuation loss factor must be added [5]. This yields

$$\overline{P_r} = \frac{P_t G_t^2 G_{nc}(n) \lambda^2 \left(\theta_B \varphi_B / \pi^2\right)(c\tau)}{1024 \ln(2) R^2 L_s \left(L_f\right)^{1/n_e}} \frac{\pi^5 |K|^2}{\lambda^4} Z \qquad (2)$$

where

L_f = single pulse fluctuation loss factor
n = number of pulses integrated
$n_e(n, \rho) = \min\left[n, 1 + (n-1)\ln(1/\rho)\right]$
ρ = correlation coefficient.

Equation (2) is the basis for computation of the basic weather detection capabilities of the MWR-05XP.

It is useful introduce signal-to-noise ratio in Eq. (2). This is accomplished simply by dividing the left side by noise power N, and the right side by noise power kT_sB to obtain

$$\left(\overline{P_r}/N\right) = \frac{P_t G_t^2 G_{nc}(n)\lambda^2\left(\theta_B\varphi_B/\pi^2\right)(c\tau)}{1024\ln(2)R^2\left(kT_sB_n\right)L_s\left(L_f\right)^{1/n_e}}\frac{\pi^5|K|^2}{\lambda^4}Z \qquad (3)$$

where

$k = 1.38\times10^{-23}$ W/Hz-°K
$T_s =$ system noise temperature in °K
$B_n =$ equivalent noise bandwidth
$\overline{P_r}/N =$ mean SNR.

(Back to Table of Contents)

B. UNAMBIGUOUS RANGE AND VELOCITY

The relations for unambiguous range and unambiguous velocity are given by [1] – [5]

$$R_u = \frac{c}{2f_p} \qquad (3)$$

and

$$v_u = \frac{\lambda f_p}{4} \qquad (4)$$

where

R_u = unambiguous range in meters
v_u = unambiguous velocity in m/s
f_p = pulse repetition frequency in Hz
λ = wavelength in meters
$c = 3\times10^8$ m/s.

Thus, the selection of PRF is a tradeoff when both target range and velocity are of interest. This is illustrated in Figure 4. (Back to Table of Contents)

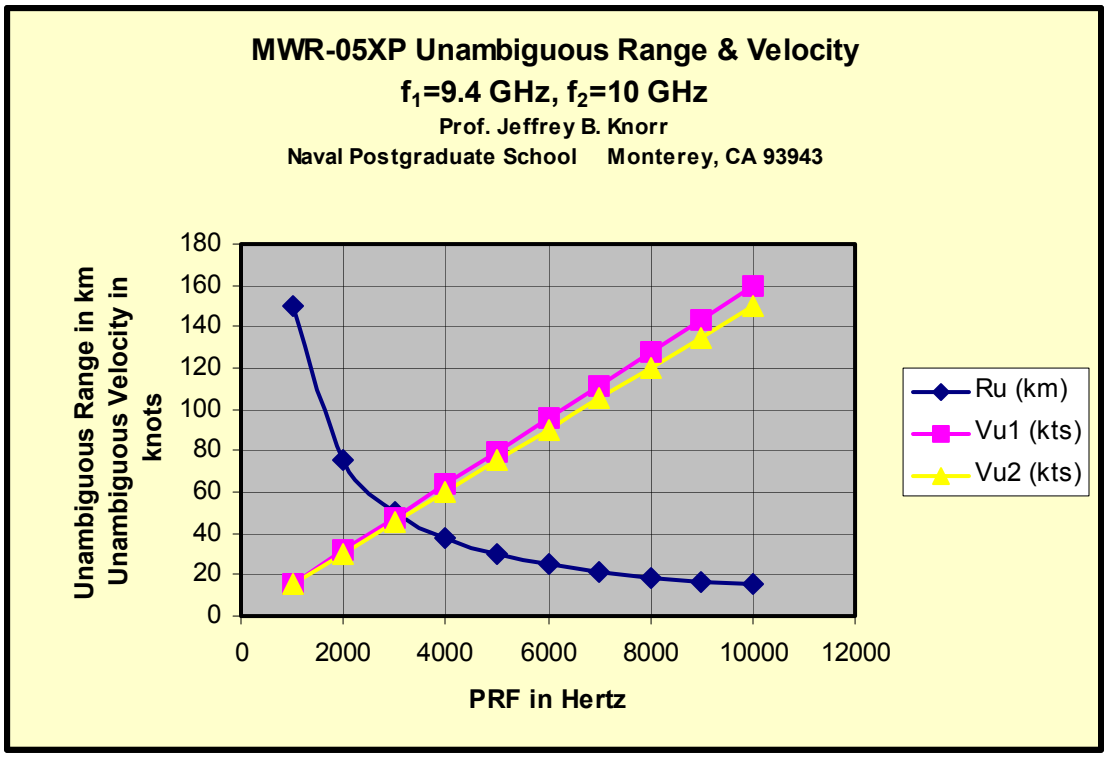

Figure 4. Unambiguous range and unambiguous velocity vs. pulse repetition frequency for the MWR-05XP radar. (Back)

It will be shown later that a PRF above 2500 Hz is generally desired for MWR-05XP velocity estimation. Figure 4 shows that unambiguous velocity is about 50 knots and unambiguous range is about 50 km for a PRF of 3 kHz. For a PRF of 10 kHz, unambiguous velocity can be increased to about 150 knots but unambiguous range drops to 15 km. (Back to Table of Contents)

C. PRECIPITATION SENSITIVITY

The sensitivity of a weather radar is often shown by computing and displaying the reflectivity level in dBZ that the radar can detect at a specified range using a single pulse with SNR = 0 dB. Figure 5 depicts the sensitivity of the MWR-05XP weather radar. The figure shows that a reflectivity of –5 dBZ can be detected at a range of 10 km while for a range of 75 km, the detectable level of reflectivity rises to about 12.5 dBZ. This is quite reasonable as a scale of 5 – 75 dBZ is normally used to display the weather return when precipitation is present. A return of 12.5 dBZ corresponds to a very light rainfall rate, approximately 0.13 mm/hr.

It is perhaps of interest to compare the sensitivity of the MWR-05 XP weather radar with that of the WSR-88D NEXRAD radar. The latter radar operates at S-band. The longer wavelength is a relative disadvantage for scattering in the Rayleigh region but this disadvantage is overcome through use of a higher gain antenna (45 dB) and higher

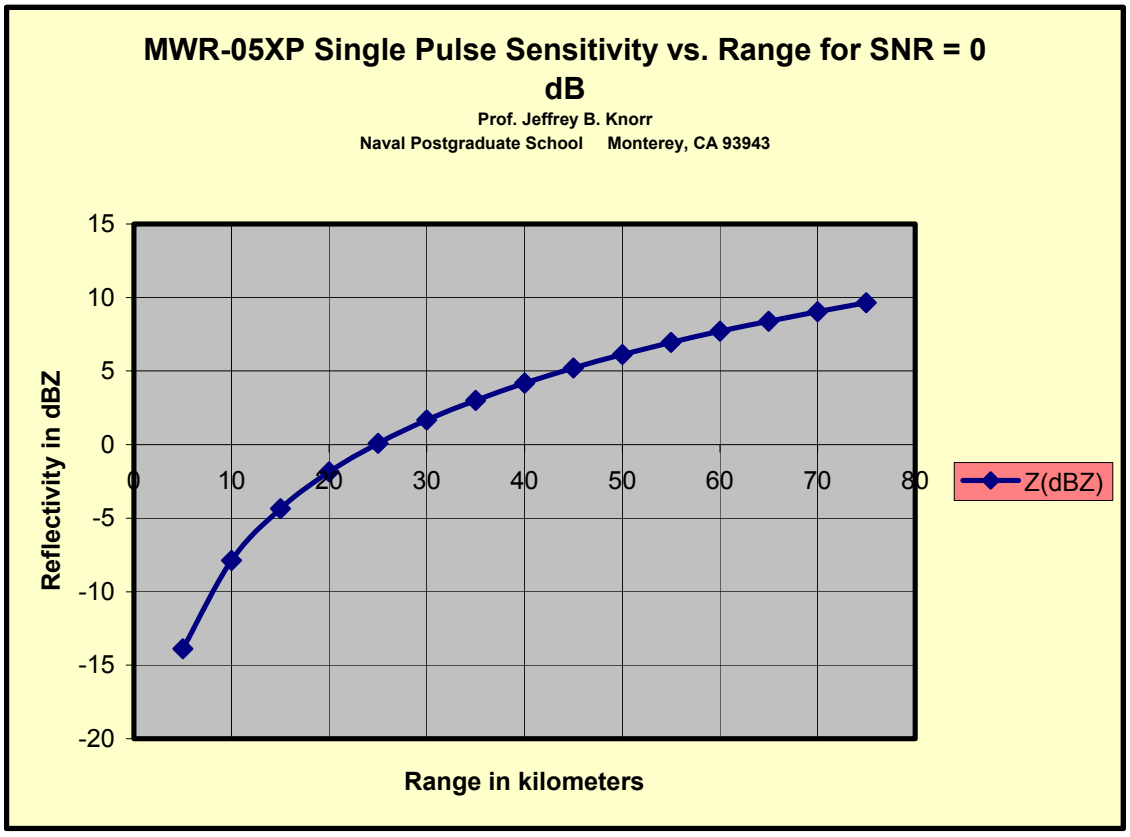

Figure 5. Single pulse reflectivity sensitivity in dBZ vs. range in km for the MWR-05XP radar. SNR = 0 dB. $Z_{dBZ} = -27.9 + 20 \log R_{km}$. (Back)

transmit power (750 kW). The WSR-88D also has a longer pulse width than that of the MWR-05XP. Figure 6 shows the sensitivities of both the MWR-05-XP and the WSR-88D. It can be seen that the the higher ERP and lower noise floor of the WSR-88D radar more than offset the disadvantage of longer wavelength, resulting in a net sensitivity advantage of about 19 dB for the WSR-88D. Although this comparison is useful because the WSR-88D is a well-known system, it should be remembered that the applications and antenna scans of the two radars are quite different. The MWR-05XP enjoys its own advantages, mobility and electronic scan. (Back to Table of Contents)

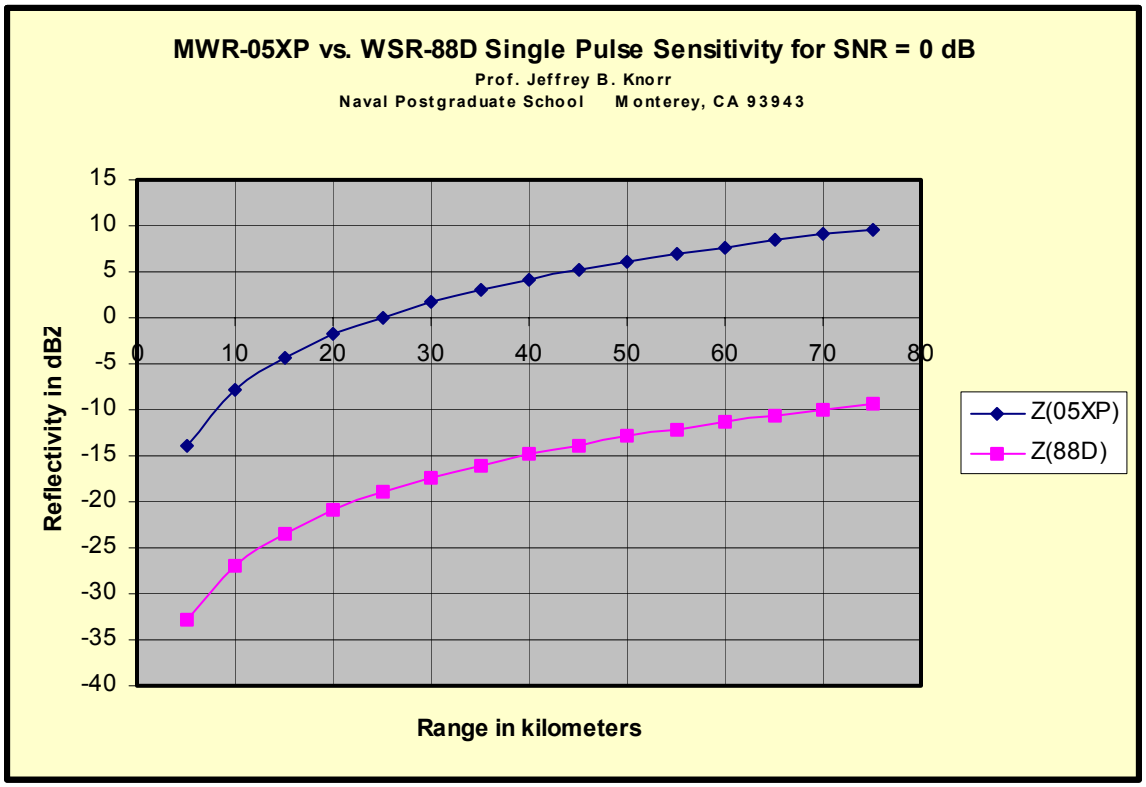

Figure 6. Single pulse reflectivity sensitivity comparison of the MWR-05XP and WSR-88D weather radars. $Z_{dBZ}^{05XP} = -27.9 + 10\log R_{km}$. $Z_{dBZ}^{88D} = -46.9 + 20\log R_{km}$. (Back)

D. PRECIPITATION PERFORMANCE

Equation (1) can be used to compute the expected value of the received signal power at the antenna output port for reflectivities of different levels and ranges. Substituting the radar system parameters in Eq. (1), one obtains

$$\overline{P_r} = -80.1 - 20\log R_{km} + Z_{dBZ} \text{ dBm.} \qquad (5)$$

A graph of received weather signal power vs. range for reflectivities between 5 and 75 dBZ is shown in Figure 7. The curves show that light precipitation will produce a return at or above the system noise floor for ranges to 45 km. For ranges less than 15-20 km., high reflectivities can result in a return that will drive the receiver into saturation. This situation would most probably occur if the radar were used to observe a tornado at short range as funnels are known to exhibit high reflectivity. It should also be remembered that individual pulses can exceed the average power level by as much as 10 dB (See Appendix 1). Thus, saturation is an issue for any reflectivity that produces average power greater than a threshold set 10 dB below the receiver saturation level or about –40 dBm. (Back to Table of Contents)

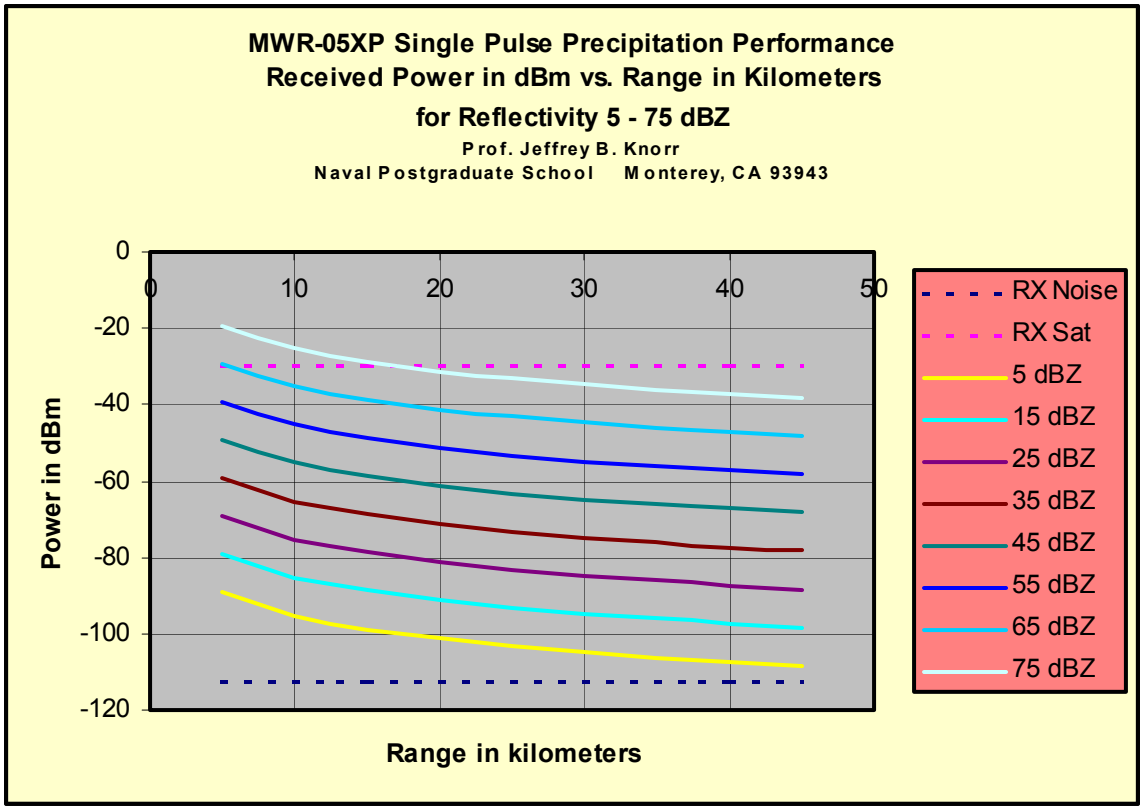

Figure 7. MWR-05XP single pulse received average power vs. range for reflectivity in the range 5 to 75 dBZ. Dashed curves show the system noise floor and receiver saturation levels. (Back)

E. BIRD AND INSECT RETURN

During periods of clear weather or in areas devoid of precipitation, radar echos generally occur due to clear air turbulence, birds or insects. It is not always easy to distinguish between these sources of return [6]. However, such return can contaminate data, especially by biasing wind velocity measurements.

The basic radar range equation can be used to calculate the echo power from insects. For the MWR-05XP, the signal power at the antenna output (receiver input) is given by

$$P_r = -74.7 + 10\log\left(\sigma_{cm^2} \Big/ R_{km}^4\right) \text{ dBm.} \qquad (6)$$

The scattering characteristics of a number of different birds and insects can be found in [5]. Typical X-band radar cross-sections are shown in Table 1.

Insect	X-Band RCS in cm^2
Aphid	10^{-5}
Mosquito	$5x10^{-4}$
Ladybug	10^{-2}
Moth	1.0
Sparrow	1.6
Grackle	16

Table 1. X-band radar cross-sections for some birds and insects. After [5]. (Back)

Using the RCS values in Table 1, the echo power for a single bird or insect can be calculated for various ranges using Eq. (6). The result is shown in Figure 8. The range of RCS in Figure 8 is 10^{-5} cm^2 to 10 cm^2; the smallest RCS value corresponding to an aphid and the largest to a big bird. It is clear that the single pulse return from a single bird or insect will generally be below the MWR-05XP system noise level and is not

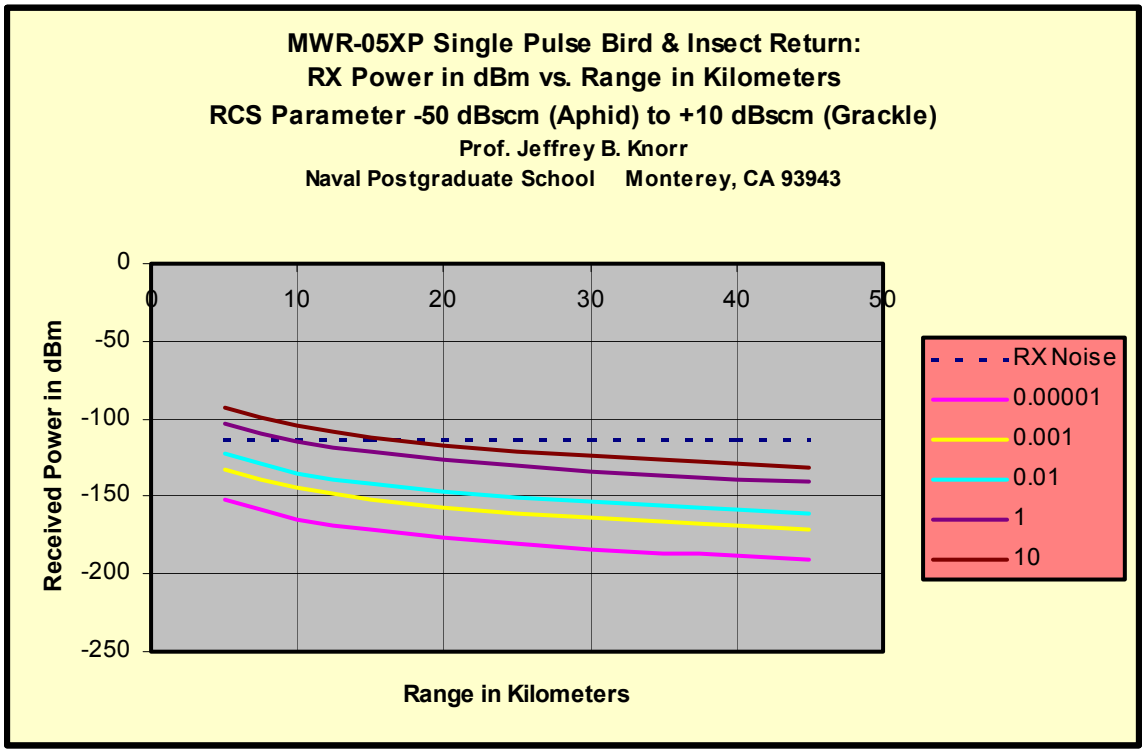

Figure 8. MWR-05XP single pulse echo power return for single birds and insects. (Back)

a concern. However, flocks of birds and insect swarms produce a much higher return and such returns are frequently observed during the summer, both day and night.

The return for flocks of birds and insect swarms is best characterized in terms of RCS density, η, in m^2/m^3. The radar range equation for this case has the form

$$P_r = \frac{P_t G_t^2 \lambda^2 \left(\theta_B \varphi_B / \pi^2\right)(c\tau)}{1024(\ln 2) R^2} \eta. \qquad (7)$$

Substituting the MWR-05XP system parameters yields

$$P_r = 35 + 10 \log \eta_{cm^2/cm^3} - 20 \log R_{km} \text{ dBm.} \qquad (8)$$

Typical RCS densities for birds and insects have been summarized by Skolnik [5]. Table 2 shows typical values of RCS density at X-band.

Type of Flock or Swarm	RCS Density, $\eta_{cm2/cm3}$
Crows, gulls, geese, ducks	$10^{-10} - 10^{-8}$
Blackbird roost	$10^{-11} - 10^{-9}$
Medium sized butterflies	$10^{-10} - 10^{-8}$
Aphid migration (major)	$10^{-9} - 10^{-8}$
All insects (1 hour)	$10^{-8} - 10^{-6}$

Table 2. X-band RCS densities for some bird flocks and insect swarms. After [5].
(Back)

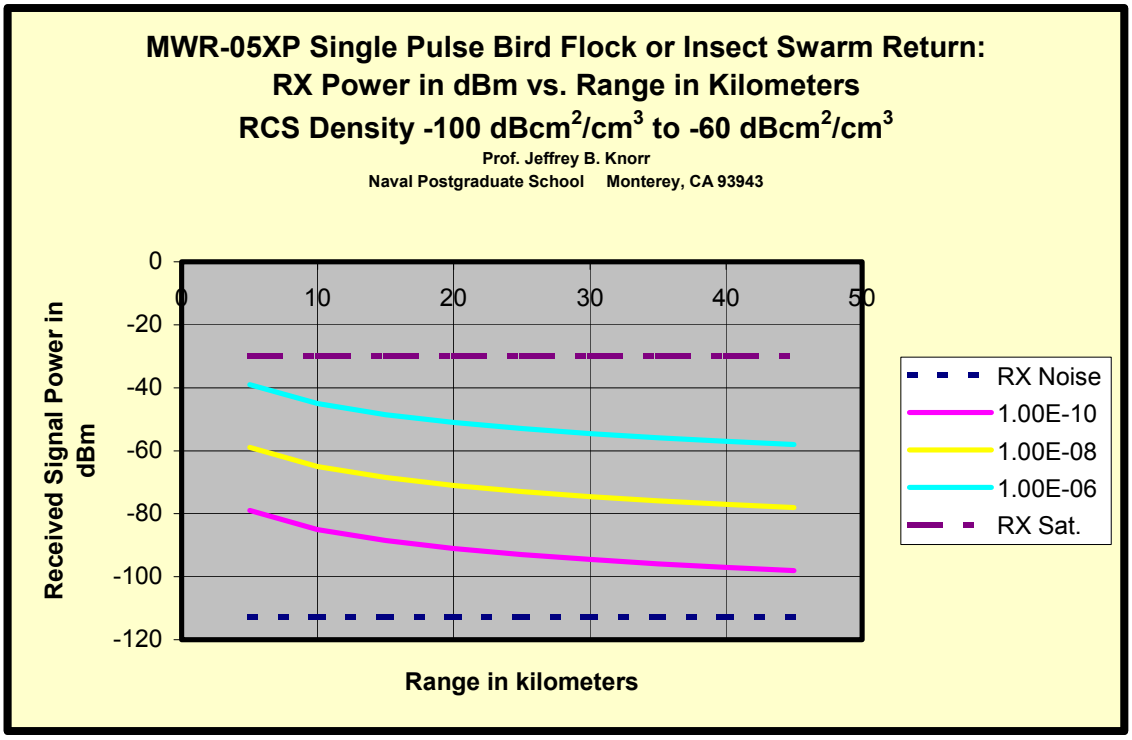

Figure 9. MWR-05XP single pulse echo signal average power vs. range for flocks of birds and swarms of insects with various RCS densities. Typical RCS densities are in the range $10^{-10} - 10^{-6}$ cm^2/cm^3. (Back)

Figure 9 shows the result obtained when the RCS densities from Table 2 are substituted in Eq. (8). The curve for $\eta = 10^{-6}$ cm^2/cm^3 results in the highest return that might be expected and corresponds to an hourly average for all insects. Birds, although they have much larger individual cross-sections, have much lower number densities and therefore would not be expected to produce a return much greater than that shown by the lowest curve in Figure 9, $\eta = 10^{-10}$ cm^2/cm^3.

The conclusion that can be drawn from Figure 9 is that insect swarms can produce a significant return at X-band. Comparing the results in Figure 9 with those in Figure 7 leads to the conclusion that insect swarms or flocks of birds can produce a return that will be displayed as a reflectivity in the range 15 – 55 dBZ. WSR-88D imagery, available on the internet, frequently shows clear air return in the lower part of the range predicted above. It should also be noted that ornithologists and entomologists use radar as a tool in their studies of birds and insects. (Back to Table of Contents)

F. CLEAR AIR PERFORMANCE

Scattering from clear air turbulence can also be observed with radar. The RCS density for clear air turbulence is [2]

$$\eta_{turb} = 0.39\lambda^{-1/3}C_n^2 \qquad (9)$$

where C_n^2 = refractive index structure parameter in m$^{-2/3}$. Typical values of the structure parameter are $C_n^2 \approx 6\times10^{-17}$ (weak) - $C_n^2 \approx 3\times10^{-13}$ (strong) [2]. Substituting Eq. (9) in the radar equation yields

$$\overline{P_r} = \frac{P_t G_t^2 \lambda^{5/3}\left(\theta_B\varphi_B/\pi^2\right)(c\tau)}{1024\left(\ln(2)\right)R^2}(0.39)C_n^2. \qquad (10)$$

Substitution of the MWR-05XP radar system parameters then yields the expression for the single pulse received signal power due to scattering from clear air turbulence,

$$\overline{P_r} = 15.9 + 10\log\left(C_n^2\right) - 20\log\left(R_{km}\right) \text{ dBm}. \qquad (11)$$

The received signal power for strong, medium and weak turbulence is shown in Figure 10. The figure shows that the return, even from strong from clear air turbulence, is more than 20 dB below the MWR-05XP system noise floor. This return is much weaker than that from insects or precipitation. Thus, during periods when no precipitation is present, return from insects and birds will normally be much greater that that from clear air turbulence. A long integration time would be required to enable observation of clear air turbulence with the MWR-05XP. Radars designed to detect clear air turbulence normally operate at much longer wavelengths, typically 10 – 20 times greater.

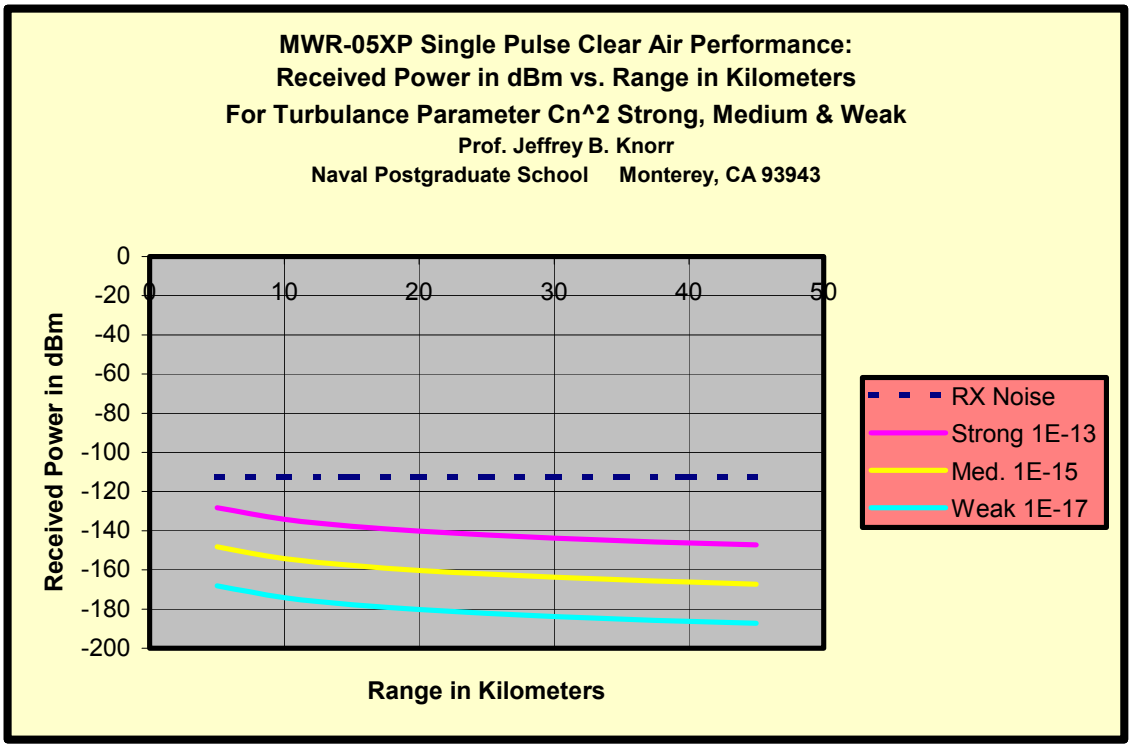

Figure 10. MWR-05XP single pulse received echo signal power vs. range for strong, medium and weak clear air turbulence. (Back)

G. FLUCTUATING TARGET INTEGRATION GAIN

Previous figures show MWR-05XP average echo power for a single pulse; for precipitation, birds, insects and clear air turbulence. Albersheim has published closed form expressions relating detection probability, P_d, false alarm probability, P_{fa}, pulses integrated, n and required SNR for non-fluctuating targets [7]. The Albersheim's equations can also be used to approximate the gain for incoherent integration of n samples [8]. Albersheim's expressions are

$$A = \ln\left[0.62/P_{fa}\right]$$
$$B = \ln\left[P_d/(1-P_d)\right]$$
$$(SNR)_1 = \chi_1 = -5\log_{10} n + \left[6.2 + \left(\frac{4.54}{\sqrt{n+0.44}}\right)\right]\log_{10}\left(A + 0.12AB + 1.7\right) \text{ dB} \qquad (12)$$
$$10^{-7} \le P_{fa} \le 10^{-3}, \qquad 0.1 \le P_d \le 0.9, \qquad 1 \le n \le 8096.$$

For the range of parameters given by Albersheim, the error in the estimate of $(SNR)_1$ is claimed to be less that 0.2 dB.

From Eq. (12), it follows that the gain for incoherent integration of n pulses is given by [8]

$$
\begin{aligned}
k &= A + 0.12AB + 1.7B \\
f(n) &= \left(\frac{0.454}{\sqrt{n + 0.44}} \right) - 0.38 \\
G_{nc}(n) &= \sqrt{n} \Big/ k^{f(n)} \qquad \text{or} \\
G_{nc}(n) &= 5 \log_{10} n - f(n) 10 \log_{10} k \text{ dB.}
\end{aligned}
\tag{13}
$$

The MWR-05XP noncoherent integration gain for a detection probability of 0.95 and a false alarm time of 1 hour is shown in Figure 11.

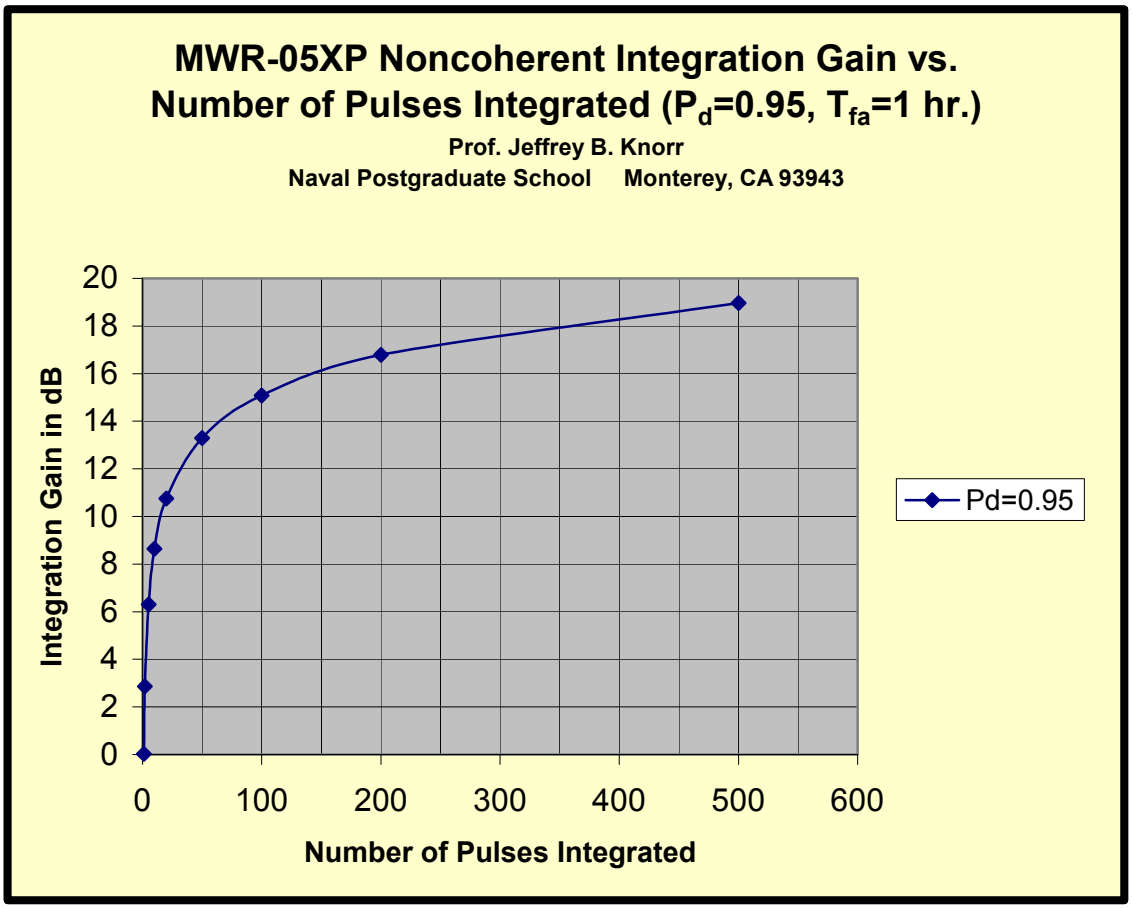

Figure 11. MWR-05XP postdetection integration gain vs. number of pulses integrated for $P_d = 0.95$, $T_{fa} = 1$ hour and an assumed nonfluctuating target. (Back)

The primary target of interest is precipitation, which produces a fluctuating echo signal return. Thus, further analysis is required to determine the integration improvement for precipitation echo pulses.

Marshall and Hitschfeld described the nature of the fluctuating return from precipitation [9]. The number and diameter of drops within the observation volume determine the average power return. The return power for a particular pulse can only be described statistically, however. Precipitation is a Rayleigh target and the echo signal power is exponentially distributed while the envelope of the detected signal voltage is Rayleigh distributed. Precipitation is thus a Swerling target of Type 1 or Type 2, depending on signal correlation [10]. Kanter [11] has determined the detection probability for a Rayleigh target when pulses are arbitrarily correlated and Shnidman [12] has provided closed form equations analogous to Albersheim's but applicable to Swerling targets of all classes. Shidman's equations are

$$
\begin{aligned}
K &= \begin{cases} \infty & \text{Swerling 0} \\ 1 & \text{Swerling 1} \\ n & \text{Swerling 2} \\ 2 & \text{Swerling 3} \\ 2n & \text{Swerling 4} \end{cases} \qquad \alpha = \begin{cases} 0 & n < 40 \\ 0.25 & n \ge 40 \end{cases} \\
\eta &= \sqrt{-0.8\ln\left(4P_{fa}\left(1-P_{fa}\right)\right)} + \operatorname{sgn}\left(P_d - 0.5\right)\sqrt{-0.8\ln\left(4P_d\left(1-P_d\right)\right)} \\
X_\infty &= \eta\left[\eta + 2\sqrt{\frac{n}{2} + \left(\alpha - 0.25\right)}\right] \\
C_1 &= \left(1/K\right)\left\{\left[\left(17.7006P_d - 18.4496\right)P_d + 14.5339\right]P_d - 3.525\right\} \\
C_2 &= \left(1/K\right)\left\{\exp\left(27.31P_d - 25.14\right) + \left(P_d - 0.8\right)\left[0.7\ln\left(10^{-5}/P_{fa}\right) + \left(2n - 20\right)/80\right]\right\} \\
C_{dB} &= \begin{cases} C_1 & 0.1 \le P_d \le 0.872 \\ C_2 + C_2 & 0.872 \le P_d \le 0.99 \end{cases} \\
C &= 10^{\left(C_{dB}/10\right)} \\
SNR &= \chi_1 = \left(CX_\infty/n\right) \\
SNR_{dB} &= 10\log_{10}\left(\chi_1\right) \\
0.1 \le P_d &\le 0.99, \qquad 10^{-9} \le P_{fa} \le 10^{-3} \qquad 1 \le n \le 100.
\end{aligned}
\tag{14}
$$

These equations are valid for a larger range of P_d and P_{fa} but a smaller range for n. Practically, however, once n exceeds the range for which the equations are valid, fluctuation loss is negligible and integration gain can be determined from Eq. (13).

It is of interest to investigate the single pulse fluctuation loss for precipitation, Swerling Case 1 ($\rho = 1$, scan-to-scan fluctuations) or Case 2 ($\rho = 0$, pulse-to-pulse fluctuations). This can be determined from Shnidman's equations and is illustrated in Figure 12.

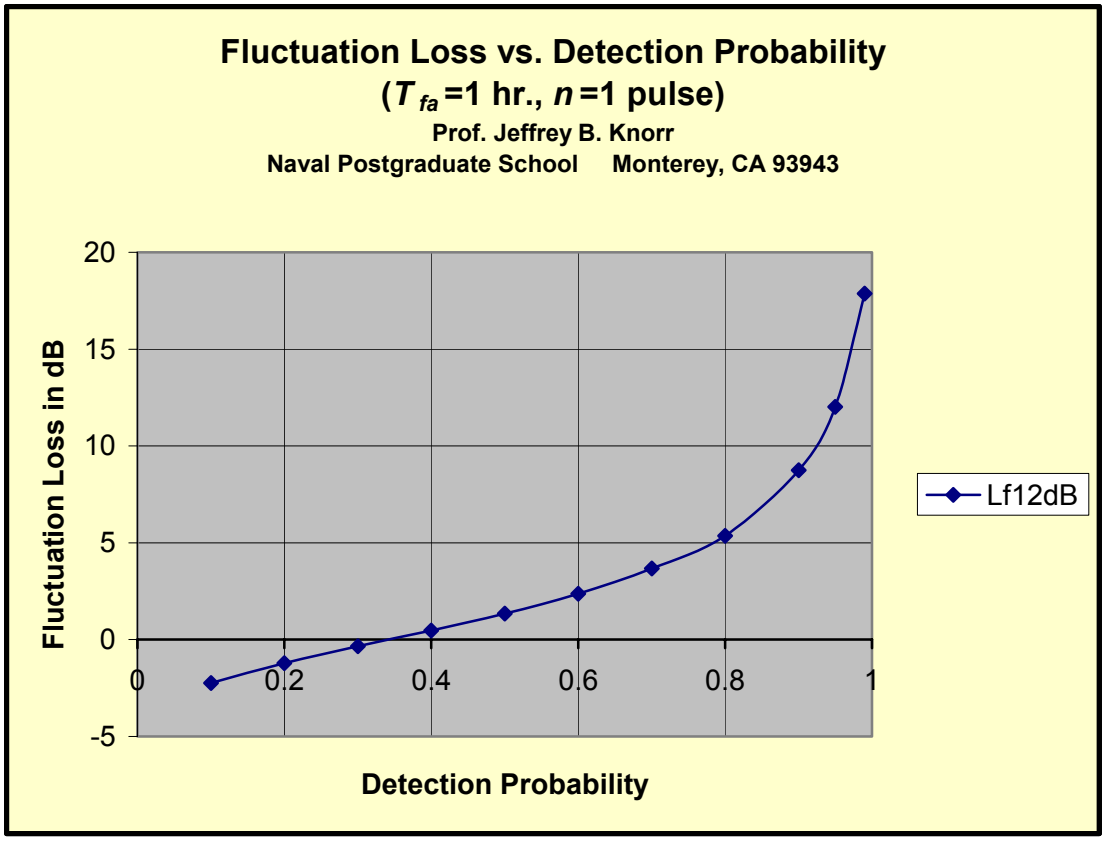

Figure 12. Fluctuation loss vs. detection probability for Swerling Type 1 and Type 2 targets. The false alarm time of 1 hour corresponds to $P_{fa} = 6.3\times10^{-10}$ for the MWR-05XP. (Back)

Fluctuation loss is the reduction in postdetection integration gain relative to a nonfluctuating target if only a single pulse is available to make the detection decision. Equivalently, fluctuation loss is the increase in single pulse SNR (relative to a nonfluctuating target) required to achieve a specified detection probability when the target echo signal power is fluctuating according to one of the Swerling models. Figure 12 shows this loss is 12 dB for a detection probability $P_d = 0.95$ and 17.9 dB for a detection probability $P_d = 0.99$.

It is interesting to note that Figure 12 shows the single pulse fluctuation loss increases as detection probability increases. For a nonfluctuating target and for fixed P_{fa}, increasing single pulse detection probability also requires an increase in SNR. Since the single pulse SNR for precipitation (a Rayleigh target) is not constant, but rather is exponentially distributed, the conclusion to be drawn is a larger single pulse SNR (relative to a nonfluctuating target) is required to assure a single precipitation echo is detected with high probability. The opposite argument holds for small detection probability. For small detection probability, a smaller single pulse SNR is required because there is a reasonable probability that a large echo signal return from precipitation will occur.

Fluctuation loss for Swerling Type 1 ($\rho = 1$) and Type 2 ($\rho = 0$) targets can be found from Figure 12 or from Shnidman's equations. According to Kanter [11], the improvement, $I_i(n)$, for incoherent integration of n pulses with correlation coefficient ρ is given by

$$n_e = \min\left[n, 1 + (n-1)\ln(1/\rho)\right]$$
$$I_i(n) = \frac{G_{nc}}{\left(L_f\right)^{(1/n_e)}} \qquad (15)$$

where L_f is the single pulse fluctuation loss, n_e is the equivalent number of independent pulses and G_{nc} is the gain for integration of n uncorrelated pulses, Eq. (13).

It is of interest to examine the effect of correlation on n_e/n. This is shown in Figure 13.

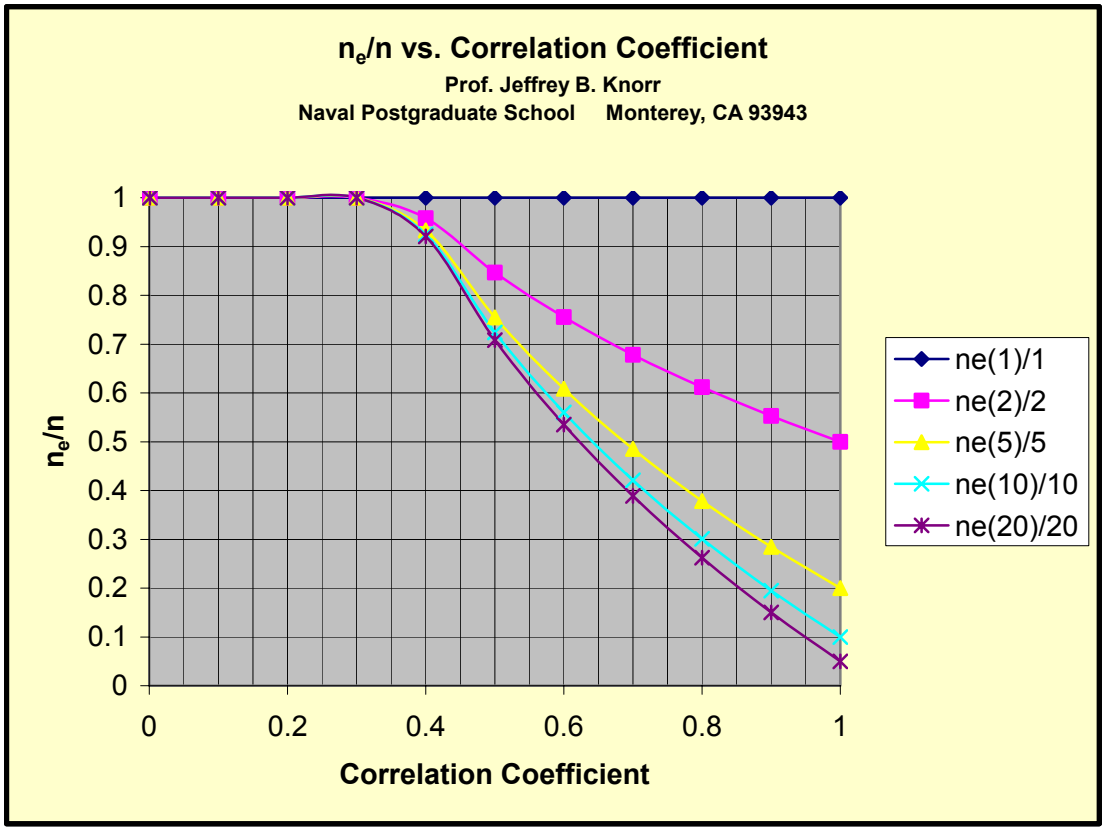

Figure 13. Effect of weather signal correlation on normalized effective number of independent pulses for one to twenty pulses received. (Back)

Figure 13 clearly shows that when the echo signal sample correlation coefficient exceeds $\rho \approx 0.4$, the effective number of independent pulses, n_e, will be less than the actual number of received pulses, n. In the limit, as $\rho \to 1$, the effective number of

independent pulses converges to $n_e = 1$, regardless of the actual number received. Thus, for a large number of received pulses, the effective fluctuation loss, $L_{fe} = \left(L_f\right)^{(1/n_e)}$, will vary from its single pulse value when $\rho = 1$, to $L_{fe} \approx 1$ (0 dB) when $\rho = 0$.

The overall integration improvement for a fluctuating target can be determined from Eq. (15) in terms of the number of pulses and their correlation. This is shown in Figures 14a – 14e.

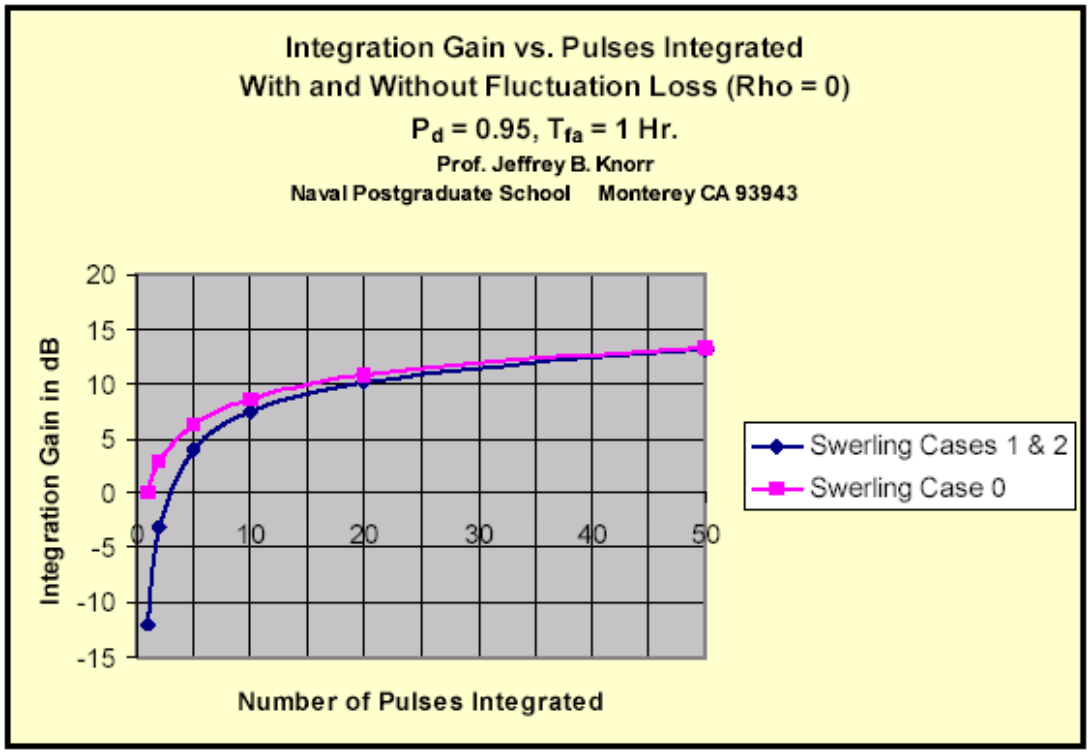

Figure 14a. Integration gain vs. pulses integrated for a detection probability, $P_d = 0.95$, false alarm probability $P_{fa} = 6.3\text{x}10^{-10}$. Pulse-to-pulse correlation is $\rho = 0$. (Back)

A conclusion that can be drawn from Figures 14a – 14e is for a specified correlation, $\rho < 1$, the integration improvement approaches that for a nonfluctuating target (Swerling Case 0) if enough pulses are integrated. Equivalently, $n_e \to n$ and the fluctuation loss, $\left(L_f\right)^{1/n_e} \to 1$ if a large number of pulses are integrated. The convergence occurs quickly for $\rho < 0.4$ and slows as $\rho \to 1$. The correlation coefficient depends on the decorrelation time for the weather signal and the radar sample interval. Signal correlation is discussed in Ch. III. (Back to Table of Contents)

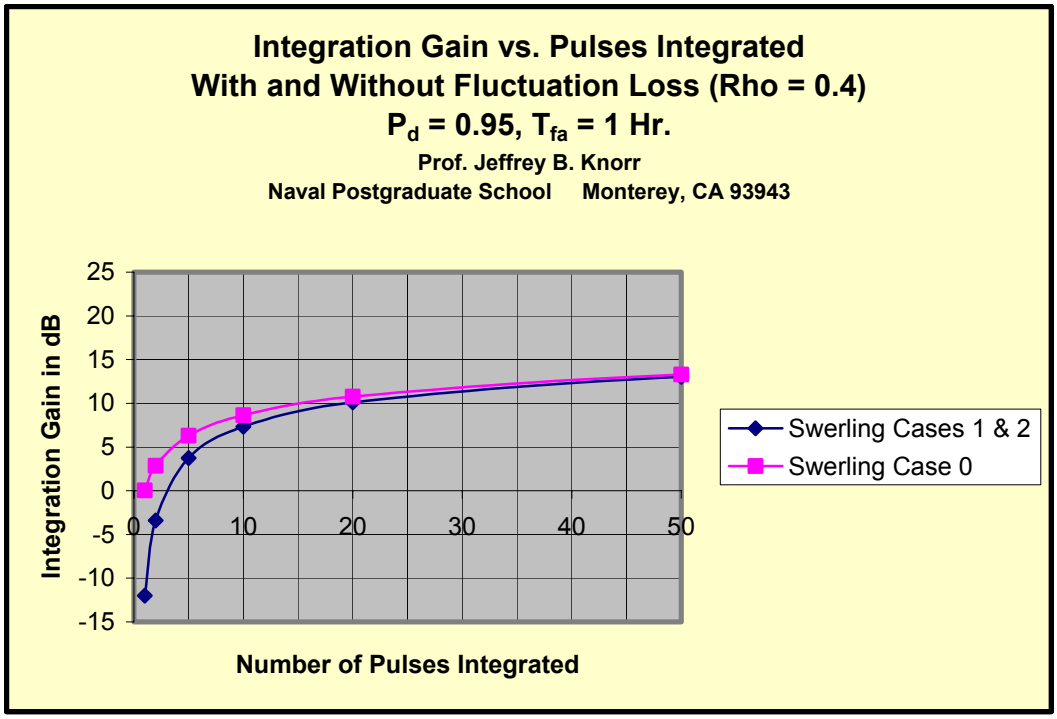

Figure 14b. Integration gain vs. pulses integrated for a detection probability, $P_d = 0.95$, false alarm probability $P_{fa} = 6.3\text{x}10^{-10}$. Pulse-to-pulse correlation is $\rho = 0.4$. (Back)

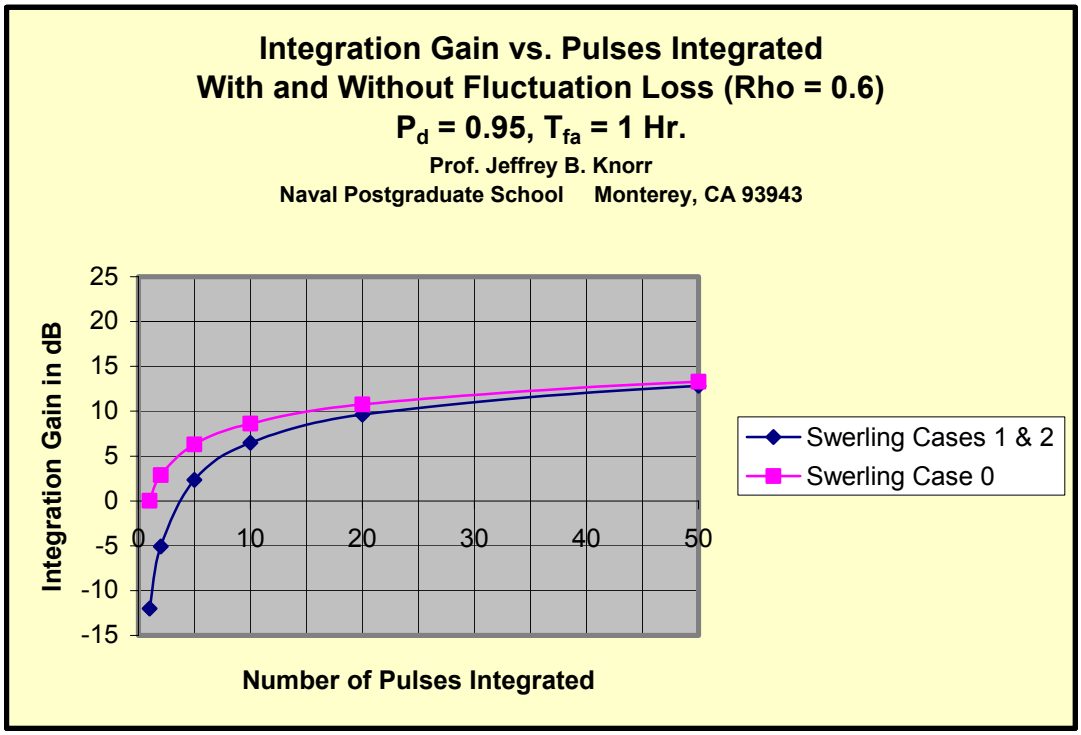

Figure 14c. Integration gain vs. pulses integrated for a detection probability, $P_d = 0.95$, false alarm probability $P_{fa} = 6.3\text{x}10^{-10}$. Pulse-to-pulse correlation is $\rho = 0.6$. (Back)

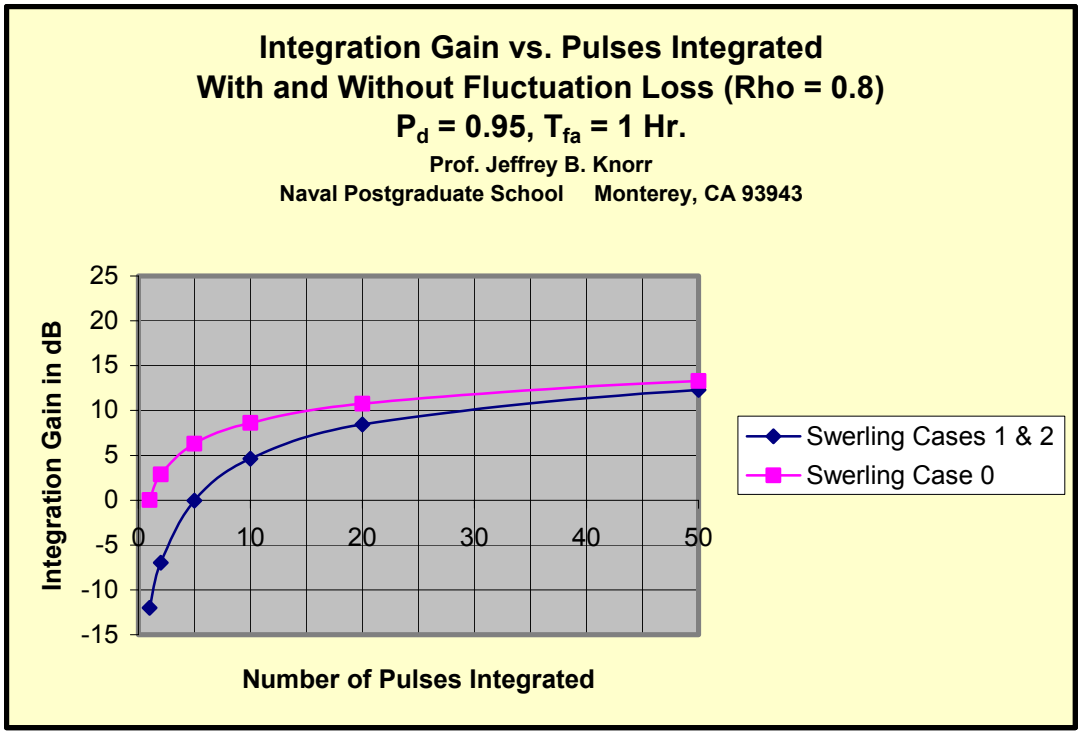

Figure 14d. Integration gain vs. pulses integrated for a detection probability, $P_d = 0.95$, false alarm probability $P_{fa} = 6.3\text{x}10^{-10}$. Pulse-to-pulse correlation is $\rho = 0.8$. (Back)

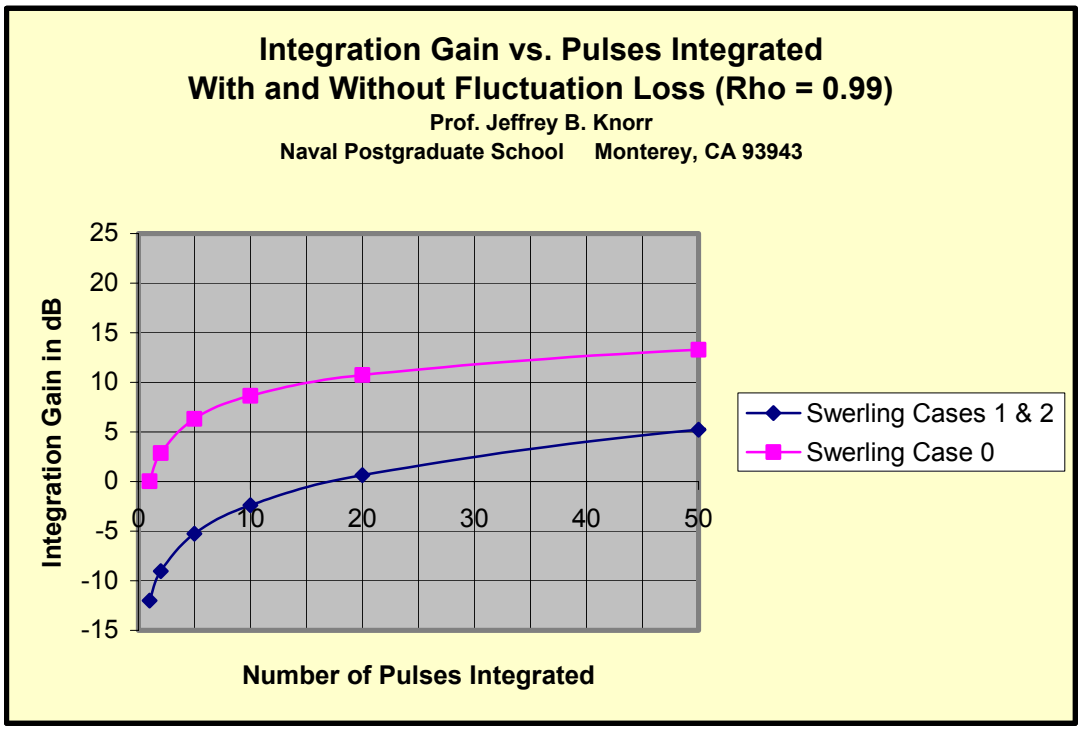

Figure 14e. Integration gain vs. pulses integrated for a detection probability, $P_d = 0.95$, false alarm probability $P_{fa} = 6.3\text{x}10^{-10}$. Pulse-to-pulse correlation is $\rho = 0.99$. (Back)

III. TEMPORAL AND SPATIAL SAMPLING STRATEGIES

A. SIGNAL CORRELATION

A weather signal is typically assumed to have a Gaussian power spectrum with spectral width σ_f determined by the rms velocity spread σ_v of the weather system. Spectral spread and velocity spread are related by $\sigma_f = 2\sigma_v/\lambda$. The weather signal autocorrelation function is found from the Fourier transform of the power spectrum. The correlation coefficient is given accordingly as (Refs. [1] – [3])

$$\rho(\tau) = e^{-\left[8\left(\frac{\pi\sigma_v\tau}{\lambda}\right)^2\right]} \qquad (16)$$

where

τ = time in seconds
σ_v = rms velocity spread in m/s
λ =.wavelength in meters.

Figure 15 shows the expected X-band weather signal correlation coefficient for parameter σ_v.

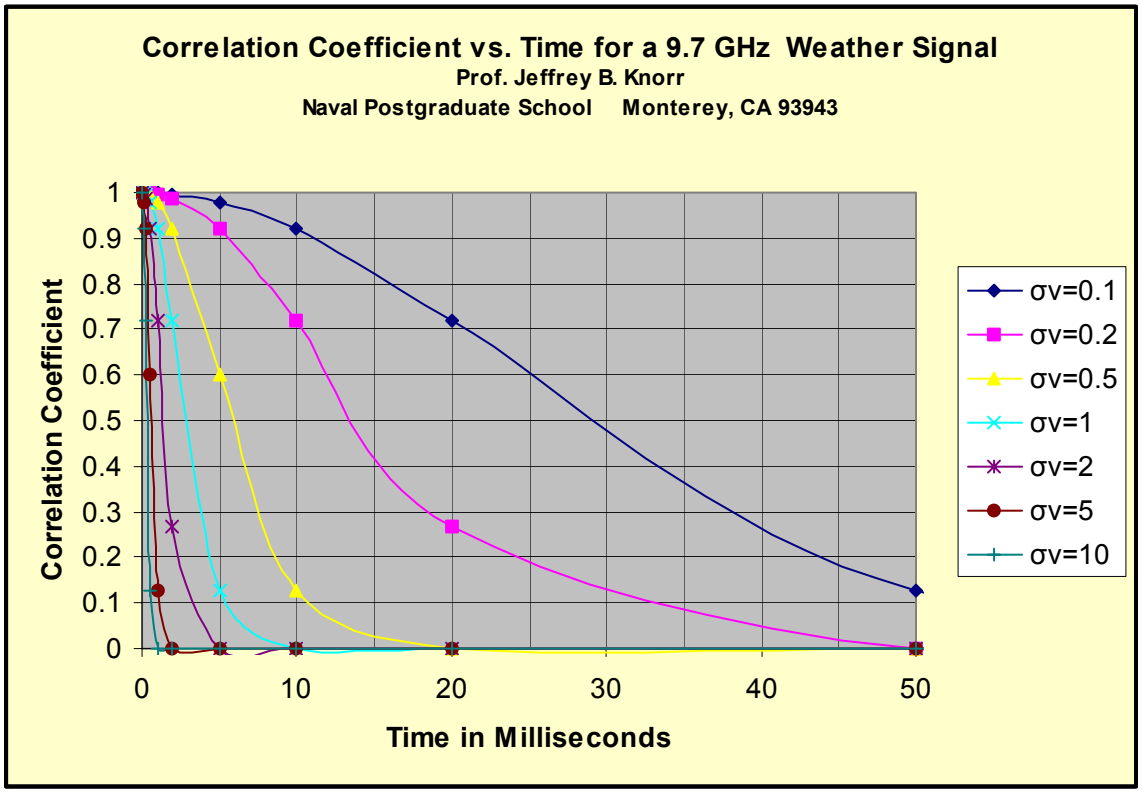

Figure 15. Correlation coefficient vs. time for a weather signal observed at f = 9.7 GHz. RMS velocity spread parameter $0.1 \text{ m/s} \le \sigma_v \le 10 \text{ m/s}$. (Back)

Of interest is the time the signal remains correlated and the time required for the signal to decorrelate. Both times depend on RMS velocity spread, σ_v. Velocity spread is a function of turbulence and wind shear.

For observations in X-band, Figure 15 shows the signal decorrelates in a time on the order of 5 – 10 milliseconds when RMS velocity spread is greater than 1 m/s. If $\rho(\tau) = e^{-4} \approx .02$ is chosen as the threshold for decorrelation, then decorrelation time can be found from Eq. (16) as

$$\tau = \left(\lambda / \sqrt{2}\pi\sigma_v\right). \qquad (17)$$

Figure 16 shows the decorrelation time obtained by applying this threshold to an X-band radar operating at 9.7 GHz.

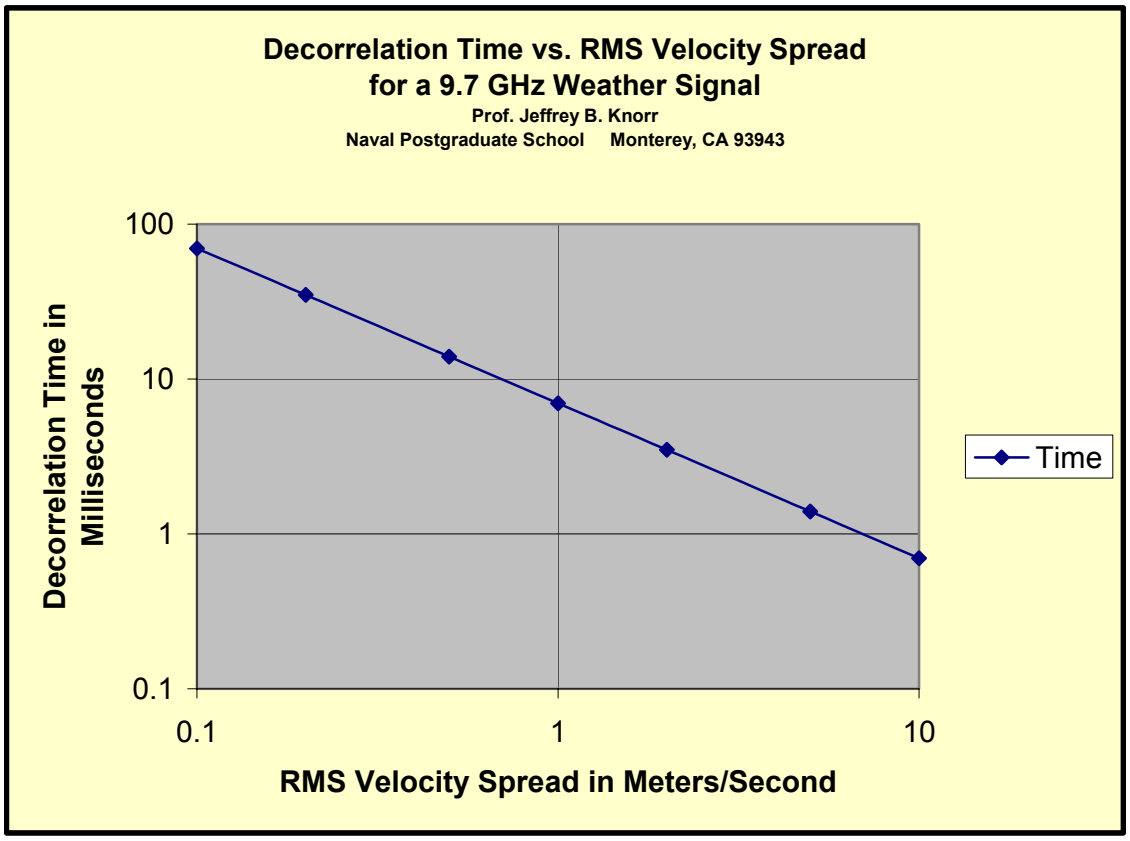

Figure 16. Decorrelation time vs. RMS velocity spread for a weather signal observed with an X-band radar. Threshold for decorrelation is assumed $\rho(\tau) = \exp(-4) \approx 0.02$. (Back)

Figure 16 shows when a weather target has RMS velocity spread $\sigma_v \geq 1$ m/s, independent weather signal samples can be obtained with an X-band radar if $T_s \geq 7$ ms where T_s is the sample time.

Also of interest is the maximum time that can elapse between samples if it is desired that the samples be highly correlated. This applies to velocity estimation where the pulse pair algorithm is used. If $\rho(\tau) = e^{-1/2} \approx 0.61$ is chosen as the threshold, then signal correlation time can be found from Eq. (16) as

$$\tau = \lambda / 4\pi\sigma_v \text{ seconds.} \qquad (18)$$

Figure 17 shows correlation time for a weather signal observed with an X-band radar.

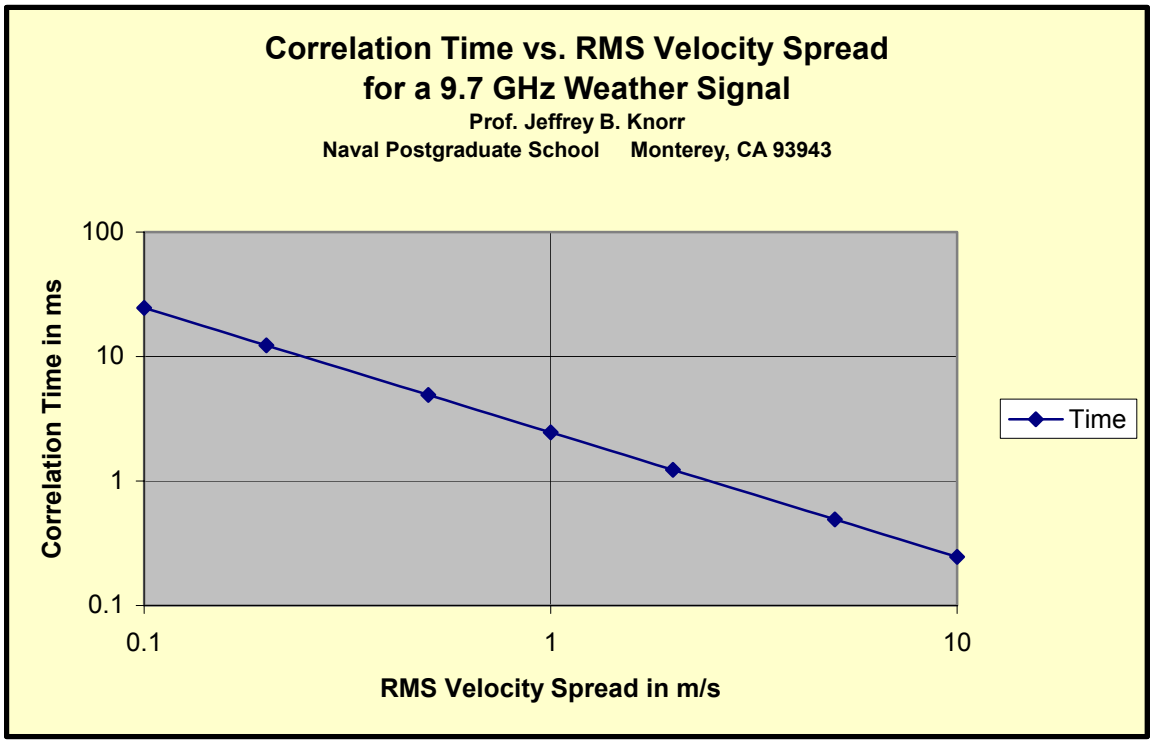

Figure 17. Correlation time vs. RMS velocity spread for a weather signal observed with an X-band radar. Threshold for correlation is assumed $\rho(\tau) = e^{-1/2} \approx 0.61$. (Back)

Research has shown that 90% of severe storms have RMS velocity spread $\sigma_v < 8$ m/s. Figure 17 shows that weather signal samples separated by no more than 0.25 ms will have high correlation if $\sigma_v < 10$ m/s. Equivalently, a pulse repetition frequency, $f_p > 2.5$ kHz will suffice for velocity estimation under most conditions. At the same time, Figure 16 shows that for $\sigma_v > 1$ m/s, 7 ms should elapse between pulse pairs to assure that independent sample pairs are obtained. An even longer time would be desirable to accommodate conditions where $\sigma_v < 1$ m/s. (Back to Table of Contents)

B. SAMPLING STRATEGY

The results of the previous section are the basis for developing an optimum sampling strategy. Here, "optimum sampling strategy" means the strategy that will both maximize volumetric update rate and minimize the variance of weather signal parameter estimates. Equivalently, it is the strategy that will result in the most rapid collection of independent sample pairs for each of the many radar beam positions (and resolution cells) of interest.

Sampling and volumetric update requirements appear conflicting. A pair of closely spaced pulses is required to estimate velocity (and avoid velocity ambiguity). As seen above, spacing should not exceed 0.25 ms. in X-band. Close spacing of pulses is consistent with a rapid volumetric update rate. However, a large number of independent sample pairs is required to estimate average velocity with small variance and this means successive sample pairs should be widely spaced in time. Successive sample pairs should be separated by at least 7 ms. in X-band; longer if velocity spread is less than 1 m/s. For a mechanically scanned radar, these requirements indeed result in a conflict. For an electronically scanned radar, they do not. Rapid volumetric update and parameter estimates with small variance can be simultaneously achieved.

The MWR-05XP uses a combination of frequency and phase control to steer the radar antenna beam electronically. Switching time for the ferrite phase shifters is in the range 90 – 100 μs. Oscillator settling time is shorter. Thus, beam steering is constrained by phase shifter switching time. It will be assumed here that 100 μs is required to change beam positions.

The MWR-05XP pulse repetition frequency is limited by the average output power capability of the TWT used in the transmitter. On a continuous basis, the maximum duty cycle of approximately 0.01 limits PRF to 10 kHz. This PRF is high enough to achieve a pulse-to-pulse correlation, $\rho(T_s) \geq 0.61$, while accommodating velocity spreads as small as $\sigma_v = 0.25$ m/s in X-band. The pulse repetition interval for this PRF is 100 μs, the same as the switching time for the phase shifters. Thus, the time required to transmit/receive two pulses and switch beam positions is 300 μs.

Consider a raster scan consisting of 200 beam positions. If a single pair of pulses separated by 0.25 ms. was transmitted in each of the 200 beam positions, an elapsed time of 60 ms would be required to scan the frame. Figure 16 shows that repeating a scan of the frame after an elapsed time of 60 ms. would result in an independent sample pair even for a velocity spread as small as $\sigma_v = 0.1$ m/s. This rapid frame scan time enables collection of a sufficient number of independent samples for computation of parameter estimates with small variance on a time scale consistent with requirements for investigation of rapidly developing storm features. (Back to Table of Contents)

C. DATA QUALITY

The sampling strategy described above allows for simple control of data quality. The desired variance of a parameter estimate can be specified and since samples are

independent, the number of samples required can be easily determined. Collecting the computed number of samples with sufficiently high SNR will then result in weather signal parameter estimates with known variance.

For example, suppose it is desired to estimate reflectivity, $\hat{Z}$, with standard deviation (*SD*), $\sigma_{\hat{Z}} \leq \pm 0.1\hat{Z}$. $\hat{Z}$ is estimated from echo signal average power, $\overline{P}$. The standard deviation for a single sample of the signal power is $\overline{P}$ (See Appendix 1 and Ref. [9]). For n independent samples the standard deviation is $\overline{P}/\sqrt{n}$. n = 100 samples will reduce the standard deviation of the average power estimate to $SD\left(\hat{\overline{P}}\right) = 0.1\hat{\overline{P}}$, thereby yielding the desired *SD* of the reflectivity estimate, $\hat{Z}$. In dBZ, this 100 sample reflectivity estimate has a standard deviation of approximately $SD\left(\hat{Z}\right) \approx \pm 0.46$ dBZ. The 2σ accuracy of the estimate is better than ± 1 dBZ. By the Central Limit Theorem, the probability the n = 100 sample reflectivity estimate is within 2σ of the true reflectivity is 0.95.

The previous example, estimating reflectivity with specified variance, requires that echo signal power be accurately measured. Thus, in the case of reflectivity, the radar must be accurately calibrated to achieve high data quality. (Back to Table of Contents)

IV. CONCLUSIONS AND RECOMMENDATIONS

A. CONCLUSIONS

Electronic scan gives the MWR-05XP radar unique capabilities as a scientific instrument for investigation of weather phenomena. This report provides performance curves that quantify the signal return expected from precipitation with varying intensity and in clear air, the return expected from birds, insects, atmospheric turbulence and wind shear. Curves are also provided to determine postdetection integration gain when fluctuation loss occurs and pulses are correlated. Lastly, sampling requirements are discussed in the context of weather signal correlation. It is shown that electronic scan enables collection of independent samples while simultaneously maintaining a rapid volumetric update rate. This is accomplished by collecting a single sample pair for each beam position in a frame, then repeating the scan of the frame to obtain another set of sample pairs that will be independent of the first set due to the signal decorrelation that occurs during the frame scan time. Both the sampling scheme and the use of frequency for beam scanning present new signal processing challenges. (Back to Table of Contents)

B. RECOMMENDATIONS

There are several areas in need of future investigation.

(1) The MWR-05XP must be calibrated to obtain accurate estimates of reflectivity. The various approaches to calibration need to be investigated and at least one approach needs to be developed and implemented for use with the MWR-05XP.

(2) The optimum sampling strategy described in this report results in data files with a different structure than those produced by a mechanically scanned radar antenna. Software must be developed to process the data in these files and compute estimates of reflectivity, average velocity and velocity spread.

(3) A third area in which interesting work could be done is data quality. It should be possible to specify a desired variance and confidence level for signal parameter estimates and use these to drive the sample collection process. This would lead to estimates of reflectivity, average velocity and velocity spread with quantified variance.

(Back to Table of Contents)

APPENDIX 1. WEATHER SIGNAL PDF

The fluctuating echo signal from precipitation has been studied by Marshall and Hitschfeld [9]. The pdf of the weather signal radar cross-section and thus the echo signal power is exponential,

$$p(P) = \frac{1}{\overline{P}} e^{-\left(P/\overline{P}\right)}. \qquad \text{(A-1)}$$

The pdf of $\log(P)$ is given by

$$p(\log P) = \frac{\exp\left\{\frac{\log P}{M} - \frac{\exp(\log P)}{\overline{P}}\right\}}{M\overline{P}}$$

where

$$M = \log_{10} e = 0.434 . \qquad \text{(A-2)}$$

Eq. (A-2) is the basis for a graph of the pdf of $\log_{10}\left(P/\overline{P}\right)$, shown in Figure 18. Of interest, is the range over which the precipitation echo signal power can be expected to vary. From Figure 18, it is clear that the instantaneous power will typically lie in the range from 30 dB below the average to 10 dB above the average. From Eq. (A-1), the probability the power exceeds the average by 6 dB is only 0.018 or slightly less than 1.8%. The probability the power exceeds the average by 10 dB is almost negligible. Thus, if a threshold is set 10 dB below the receiver saturation level, precipitation return with average echo signal power at or below this threshold will not produce any echos that drive the receiver into saturation.

For the MWR-05XP, the threshold described above would be about -40 dBm. From Figure 7, it is evident that if reflectivity is below 55 dBZ, the receiver will operate linearly for all ranges greater than 5 km. (Back to Table of Contents)

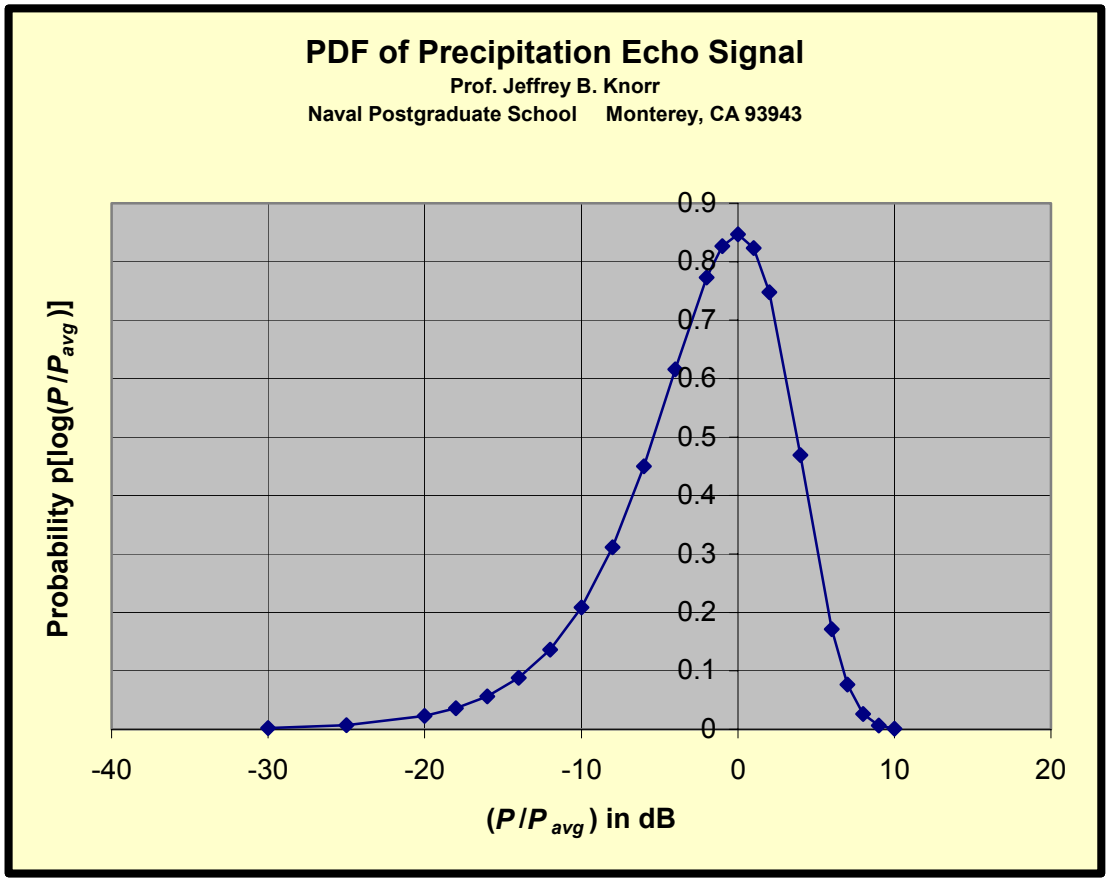

Figure 18. PDF of precipitation echo signal power. P is the instantaneous power and P_{avg} is the expected value of the echo signal power. (Back)

APPENDIX 2. MWR-05XP SYSTEM PARAMETERS

Effective Radiated Power (measured)	109.7 dBm
Pulse Width (measured)	1.0 μs
PRF	10 kHz (max.)
Frequency	X-band
Azimuth Beamwidth	1.8 degrees
Elevation Beamwidth	2.0 degrees
Phase Shifter Switching Time	100 μs
System Noise Floor (measured)	-112.8 dBm
Receiver Saturation Level (measured at RX input)	-30 dBm

(Back to Table of Contents)

REFERENCES

[1] *Doppler Radar Meteorological Observations, Part B, Doppler Radar Theory and Meteorology*. FCM-H11B-1990, U.S. Department of Commerce, NOAA, June 1990. http://www.ncdc.noaa.gov/oa/radar/radarresources.html.

[2] Doviak, R.J. and D.S. Zrnic, *Doppler Radar and Weather Observations*. ISBN 0-12-221422-6, Second edition, Academic Press, 1993. (http://www.academicpress.com).

[3] H. Sauvageot, *Radar Meteorology*. ISBN 0-89006-318-4, Arthech House, Inc., 1992.

[4] R. Rinehart, *Radar for Meteorologists*. ISBN 0-9658002-0-2, Rinehart Publications, 1997. http://www.radarwx.com/

[5] M. I. Skolnik, *Introduction to Radar Systems*. ISBN 0-07-290980-3, Third edition, McGraw-Hill, 2001.

[6] William Martin, "*Measurements and Modeling of the Great Plains Low-Level Jet*", Ph.D. dissertation, University of Oklahoma, 2003.

[7] W. Albersheim, "Closed form approximation to Robertson's detection characteristics", *Proceedings of IEEE*, Vol. 69, No. 7, p 839, July 1981.

[8] M. A. Richards, *Fundamentals of Radar Signal Processing*. ISBN 0-07-144474-2, McGraw-Hill, 2005.

[9] J. Marshall and W. Hitschfeld, "Interpretation of the fluctuating echo from randomly distributed scatterers. Part I", *Canadian Journal of Physics*, Vol. 31, pp. 962-993, 1953.

[10] P. Swerling, "Probability of detection for fluctuating targets", *IRE Transactions*. IT-6, pp. 269-308, April 1960.

[11] I. Kanter, "Exact detection probability for partially correlated Rayleigh targets", *IEEE Trans. Aerospace and Electronic Systems*, Vol. AES-22, pp184-189, March 1986.

[12] D. Shnidman, "Determination of Required SNR Values", *IEEE Trans. Aerospace and Electronic Systems*, Vol. 38, No. 3, pp1059-1064, July 2002.

(Back to Table of Contents)

INITIAL DISTRIBUTION LIST

1. Defense Technical Information Center
   Ft. Belvoir, Virginia
   (800) 225-3842

2. Dudley Knox Library
   Naval Postgraduate School
   Monterey, California 93943

3. Prof. Jeffrey B. Knorr
   Room 428 Spanagel Hall
   Naval Postgraduate School
   Monterey, CA 93943

4. Ivan PopStefanija, Vice President
   ProSensing, Inc.
   107 Sunderland Road
   Amherst, MA 01002-0198

5. Bob Bluth, Director
   Center for Interdisciplinary Remotely Piloted Aircraft Studies (CIRPAS)
   Research Office (Code 093)
   Naval Postgraduate School
   Monterey, CA 93943

6. Prof. Chuck Wash
   Room 254 Root Hall
   Department of Meteorology
   Naval Postgraduate School
   Monterey, CA 93943

7. Paul Buczynski, Staff Director
   Radar Laboratory (Code EC)
   Department of Electrical and Computer Engineering
   Naval Postgraduate School
   Monterey, CA 93943